

**EVALUATION OF THE EFFECT OF CYCLIC LOAD ON THE
MICROGAP AT THE IMPLANT-CAST ABUTMENT
INTERFACE OF SCREW-RETAINED IMPLANT SUPPORTED
RESTORATIONS**

Dissertation Submitted to
THE TAMILNADU DR. M.G.R. MEDICAL UNIVERSITY

In partial fulfillment for the Degree of
MASTER OF DENTAL SURGERY




**BRANCH I
PROSTHODONTICS AND CROWN & BRIDGE
APRIL 2013**


CERTIFICATE

This is to certify that the dissertation titled “EVALUATION OF THE EFFECT OF CYCLIC LOAD ON THE MICROGAP AT THE IMPLANT-CAST ABUTMENT INTERFACE OF SCREW-RETAINED IMPLANT SUPPORTED RESTORATIONS” is a bonafide record work done by Dr. Soumya Ray under our guidance and to our satisfaction during his post graduate study period between 2010 – 2013.


This dissertation is submitted to THE TAMILNADU Dr. M.G.R. MEDICAL UNIVERSITY, in partial fulfillment for the Degree of MASTER OF DENTAL SURGERY – PROSTHODONTICS AND CROWN & BRIDGE, BRANCH I. It has not been submitted (partial or full) for the award of any other degree or diploma.

GUIDED BY:


Dr. N.S. Azhagarasan, M.D.S.,
Professor and Head of the Department,
Department of Prosthodontics and
Crown & Bridge,
Ragas Dental College & Hospital,
Chennai.


Dr. K. Chitra Shankar, M.D.S.,
Professor,
Department of Prosthodontics and
Crown & Bridge,
Ragas Dental College & Hospital,
Chennai.

PROFESSOR & HEAD
DEPT. OF PROSTHODONTICS
AND CROWN & BRIDGE
Ragas Dental College & Hospital
Chennai - 600 119.


Dr. S. Ramachandran, M.D.S.,
Principal,
Ragas Dental College & Hospital,
Chennai.

PRINCIPAL
RAGAS DENTAL COLLEGE & HOSPITAL
CHENNAI

PROFESSOR
DEPT. OF PROSTHODONTICS
AND CROWN & BRIDGE
Ragas Dental College & Hospital
Chennai - 600 119.

ACKNOWLEDGEMENT

This dissertation is the result of work with immense support from many people and it is a pleasure now that I have the opportunity to express my gratitude to all of them.

*I would be failing in my duty if I do not adequately convey my heartfelt gratitude and my sincere thanks to my Head of the Department, **Professor Dr. N.S. Azhagarasan, M.D.S.**, Department of Prosthodontics and Crown & Bridge, Ragas Dental College and Hospital, Chennai, for his exceptional guidance, tremendous encouragement, well-timed suggestions and heartfelt support throughout my postgraduate programme, which has never failed to drive the best out of me. I would like to profoundly thank him for giving an ultimate sculpt to this study. I will remember his help for life.*

*I wish to express my gratitude to **Dr. S. Ramachandran, M.D.S.**, **Principal**, Ragas Dental College and Hospital, Chennai, for his encouragement throughout my postgraduate course. I also thank him for permitting me to make use of the amenities in the institution.*

*I would like to express my real sense of respect, gratitude and thanks to my **Guide, Professor Dr. K. Chitra Shankar M.D.S.**, for her guidance, constant support, back up and valuable criticism extended to me during the period of my study. The timely help and encouragement rendered by her has been enormously helpful throughout the period of my postgraduate study.*

*I would like to solemnly thank **Dr. R. Hariharan, M.D.S., Reader**, for the valuable guidance and encouragement rendered by him. This dissertation has been the fertile outcome of his massive endurance, support, proficient guidance and counsel.*

*I would also like to thank **Dr. K. Madhusudan, M.D.S., Dr. S. Jayakrishnakumar, M.D.S., Dr. Manoj Rajan, M.D.S., Dr. Saket Miglani, M.D.S., Dr. M. Saravana Kumar, M.D.S., Dr. Sabarinathan. M.D.S., Dr. Vallabh Mahadevan, M.D.S. and Dr. Divya Krishnan, M.D.S.**, for their valuable suggestions and help given throughout my study.*

*I would also like to thank all the staff members at **Central Workshop, Dept. of Manufacturing Engineering, Anna University, Chennai** for extending their support and expertise in the measurement phase of my study.*

*I thank **Ms. R. Deepa**, Statistician, Ragas Dental College and Hospital for helping me with the statistical analysis of this study.*

*It would not be justifiable on my part if I do not acknowledge the help of my **fellow colleagues, seniors and juniors**, for their criticism and continuous support throughout my postgraduate course.*

*I wish to thank my wife **Dr. Swetha Ray, B.D.S.** for her unstinted support, care and encouragement in all walks of my life and her constant motivation throughout the period of my study.*

*Last but not the least, even though words wouldn't do much justice, I would like to specially thank my parents **Mr. Bikas Ray** and **(Late) Mrs. Maitreyee Ray** and my grandparents **Mr. U. P. Chattopadhyay** and **(Late) Mrs. Manashi Chattopadhyay** for their blessings and unconditional love.*

*Above all I thank **GOD** almighty for all the grace endowed upon me.*

CONTENTS

S.NO	TITLE	PAGE NO.
1.	INTRODUCTION	1
2.	REVIEW OF LITERATURE	8
3.	MATERIALS AND METHODS	22
4.	RESULTS	39
5.	DISCUSSION	52
6.	CONCLUSION	66
7.	SUMMARY	69
8.	BIBLIOGRAPHY	71

LIST OF TABLES

Table No.	Title	Page No.
I	Basic values and mean microgap at the implant-cast abutment interface of Group I samples (Ni-Cr) before cyclic loading	42
II	Basic values and mean microgap at the implant-cast abutment interface of Group I samples (Ni-Cr) after cyclic loading	43
III	Basic values and mean microgap at the implant-cast abutment interface of Group II samples (Co-Cr) before cyclic loading	44
IV	Basic values and mean microgap at the implant-cast abutment interface of Group II samples (Co-Cr) after cyclic loading	45
V	Comparison between mean values of microgap at implant-cast abutment interface of Group I samples (Ni-Cr) before and after cyclic loading using Paired 't'-Test	46
VI	Comparison between mean values of microgap at implant-cast abutment interface of Group II samples (Co-Cr) before and after cyclic loading using Paired 't'-Test	47
VII	Comparison between mean values of microgap of Group I (Ni-Cr) and Group II (Co-Cr) samples at implant-cast abutment interface before cyclic loading using Independent 't'-Test	48
VIII	Comparison between mean values of microgap of Group I (Ni-Cr) and Group II (Co-Cr) samples at implant-cast abutment interface after cyclic loading using Independent 't'-Test	49
IX	Overall comparison between mean values of microgap at implant-cast abutment interface of Group I (Ni-Cr) and Group II (Co-Cr) samples before and after cyclic loading	50

ANNEXURE

LIST OF FIGURES

FIG.NO.	TITLE
Fig.1:	Non-surface treated titanium dental implant, 3.75 X 11.50 mm
Fig.2:	Spirit level indicators
Fig.3:	Clear autopolymerizing acrylic resin
Fig.4a:	Direct plastic cylinder internal hex with hex
Fig.4b:	Titanium abutment screw
Fig.5a:	1.25 mm Hex drive, Long
Fig.5b:	Calibrated torque wrench
Fig.6a:	Soft putty, Polyvinyl siloxane impression material-Addition type
Fig.6b:	Light body, Polyvinyl siloxane impression material-Addition type
Fig.6c:	Auto mixing spiral
Fig.6d:	Auto mixing gun
Fig.7:	Inlay casting wax
Fig.8:	PKT Instruments

- Fig.9a:** Sprue wax
- Fig.9b:** Surfactant spray
- Fig.9c:** Silicone investment ring and crucible former
- Fig.9d:** Phosphate bonded investment
- Fig.9e:** Colloidal silica
- Fig.9f:** Distilled water
- Fig.9g:** Paint brush
- Fig.10:** Nickel-Chromium (Ni-Cr) alloy pellets
- Fig.11:** Cobalt-Chromium (Co-Cr) alloy pellets
- Fig.12a:** Casting crucible
- Fig.12b:** Aluminium oxide powder
- Fig.13a:** Carborundum separating discs
- Fig.13b:** Tungsten carbide burs
- Fig.13c:** Silicon carbide rubber points
- Fig.14a:** Plastic instrument
- Fig.14b:** Light cure restorative composite
- Fig.15:** Custom-made jig

- Fig.16:** Dental surveyor
- Fig.17:** Vacuum power mixer
- Fig.18a:** Burnout furnace
- Fig.18b:** Induction casting machine
- Fig.19:** Sandblaster
- Fig.20:** Alloy grinder
- Fig.21:** Light cure unit
- Fig.22:** Scanning Electron Microscope
- Fig.23a:** Custom-made cyclic loading machine
- Fig.23b:** Line diagram for custom-made cyclic loading machine
- Fig.24a:** Custom-made stainless steel block
- Fig.24b:** Line diagram of custom-made stainless steel block
- Fig.25:** Custom made stabilizing plates
- Fig.26:** Surveying platform made parallel to floor using spirit level indicators
- Fig.27:** Stabilized stainless steel block
- Fig.28:** Positioning of titanium implant in stainless steel block
- Fig.29:** Autopolymerizing clear acrylic resin poured in the mold space

- Fig.30:** Implant placed in clear acrylic resin
- Fig.31:** Connecting direct plastic cylinder to implant
- Fig.32a:** Screw access hole closed with putty polyvinyl siloxane
- Fig.32b:** Wax-up on plastic cylinder
- Fig.33:** Cingulum contoured to flat surface at 30° to long axis of tooth
- Fig.34a:** Index for duplicating the wax patterns
- Fig.34b:** Index for duplicating the wax patterns (inside view)
- Fig.35a:** Pattern attached to crucible former
- Fig.35b:** Investing the pattern
- Fig.35c:** Burnout procedure
- Fig.35d:** Casting procedure
- Fig.36a:** Completed casting with button
- Fig.36b:** Partially cleaned casting
- Fig.36c:** Sandblasted casting
- Fig.36d:** Casting after sprue sectioning
- Fig.36e:** Completed restoration (i&ii) and prosthetic screw (iii)
- Fig.37:** Fixation of cast abutment-restoration using calibrated torque wrench

- Fig.38a:** Light cure restorative composite filled into screw access hole
- Fig.38b:** Light cure composite cured
- Fig.39a:** Group I test samples - Ni-Cr cast abutment-restorations
- Fig.39b:** Group II test samples - Co-Cr cast abutment-restorations
- Fig.40a&b:** Implant-cast abutment interface (Ni-Cr)
- Fig.40c&d:** Implant-cast abutment interface (Co-Cr)
- Fig.41a:** Measurement of microgap at implant-cast abutment interface before cyclic loading of Group I (Ni-Cr) using Scanning Electron Microscope (S.E.M.)
- Fig.41b:** Measurement of microgap at implant-cast abutment interface before cyclic loading of Group II (Co-Cr) using S.E.M.
- Fig.42a:** Stylus placed on flattened cingulum of test sample
- Fig.42b:** Cyclic loading of the test sample
- Fig.43a:** Measurement of microgap at implant-cast abutment interface after cyclic loading of Group I (Ni-Cr) using S.E.M.
- Fig.43b:** Measurement of microgap at implant-cast abutment interface after cyclic loading of Group II (Co-Cr) using S.E.M.
- Fig.44a&b:** Comparative S.E.M. pictures (Ni-Cr)
- Fig.45a&b:** Comparative S.E.M. pictures (Co-Cr)

LIST OF GRAPHS

Graph No.	Title
I	Basic values of microgap at implant-cast abutment interface for Group I samples (Ni-Cr) before cyclic loading
II	Basic values of microgap at implant-cast abutment interface for Group I samples (Ni-Cr) after cyclic loading
III	Basic values of microgap at implant-cast abutment interface for Group II samples (Co-Cr) before cyclic loading
IV	Basic values of microgap at implant-cast abutment interface for Group II samples (Co-Cr) after cyclic loading
V	Comparison between mean values of microgap at the implant-cast abutment interface of Group I samples (Ni-Cr) before and after cyclic loading
VI	Comparison between mean values of microgap at the implant-cast abutment interface of Group II samples (Co-Cr) before and after cyclic loading
VII	Comparison between mean values of microgap of Group I (Ni-Cr) and Group II (Co-Cr) samples at implant-cast abutment interface before cyclic loading
VIII	Comparison between mean values of microgap of Group I (Ni-Cr) and Group II (Co-Cr) samples at implant-cast abutment interface after cyclic loading
IX	Overall comparison between mean values of microgap at implant-cast abutment interface of Group I (Ni-Cr) and Group II (Co-Cr) samples before and after cyclic loading

ABSTRACT

Background: Comparative literature on the effect of cyclic loading, on the microgap at the implant-cast abutment interface of screw-retained implant supported restoration using base metal alloys are inadequately documented.

Materials and methods: Ten implant-supported cast abutment-restorations each were fabricated using Nickel-Chromium (Ni-Cr) (Group I) and Cobalt-Chromium (Co-Cr) alloy (Group II). All twenty samples were subjected to cyclic loading of 0-109N, for 1,50,000 cycles, simulating 6 months of function. Scanning electron microscopic measurements of the implant-cast abutment interface were made both before and after cyclic loading. The results were analyzed using Paired 't' and Independent 't' test.

Results: Cyclic loading resulted in the reduction of the microgap at the implant-cast abutment interface for both Ni-Cr and Co-Cr test samples. The respective differences between the mean pre and post cyclic load microgap measurements for both groups were statistically insignificant (p -value > 0.05). Whereas, the mean microgap values after cyclic loading were significantly lower than those values before cyclic loading for both Ni-Cr and Co-Cr samples (p -value < 0.05).

Conclusion: Simulated functional loading on a maxillary anterior screw-retained implant-supported restoration led to a decrease in the microgap at the implant-cast abutment interface.

Keywords: Screw-retained implant-supported restorations, cast-abutment restorations, implant-cast abutment interface, microgap.

INTRODUCTION

Osseointegrated titanium dental implants have been used extensively in oral rehabilitation for the replacement of one or more missing teeth, with satisfactory survival rates.^{1,2,7,29,38} With a reported long-term success rates of above 90%, implant-supported prostheses have enabled patients to experience a satisfactory resolution of their prosthodontic problems.^{1,11,53} The treatment option of single-tooth implant-supported restorations is now largely accepted with satisfactory outcomes from longitudinal studies reported in the literature.¹³

Currently, a majority of partially edentulous situations restored with single-tooth implant-supported restoration employ a two-piece endosseous implant and its transmucosal component, joined together by the clamping action of abutment screw joint.¹¹ Implant restorations over such two-piece implants can be cement-retained, screw-retained, or a combination of both. Even though, cement-retained prostheses provides a less costly and simpler method of fabrication, their use in the anterior single-tooth situation may be restricted due to implant angulation and esthetic requirements.^{27,35}

The use of screw-retained implant prostheses in restoring completely and partially edentulous patients is well documented.^{2,35} They are advocated in partially edentulous situations to overcome angulation and esthetic problems.^{7,8} They provide an advantage of retrievability of restorations for

reservicing and/or replacement of the restoration.³⁵ It is also reported that these prostheses have exhibited significantly smaller marginal opening as compared to cement-retained restorations.²⁷

Although screw-retained crown protocol for a single-tooth two-piece implant, is well established, crown complications are common.^{10,27} These complications are mostly associated with implant-abutment screw joint integrity.¹⁵ This joint is also known as the implant-abutment interface. This can be either a butt-joint or a bevel joint.⁷ The contact between implant and abutment platform is a key factor, as it reduces the load over the abutment or prosthesis screw.⁸ Poor adaptation or misfit at the implant-abutment interface gives rise to a marginal gap between the implant and the abutment. Loss of integrity of this joint or interface leads to biologic, mechanical or both types of complications.^{8,25,27}

The screw-type connections (both external and internal hexagon types) rely on clamping the abutment to the top of the implant by a connecting screw, torqued to pre-determined values as established by the implant manufacturer.¹¹ This clamping force between two surfaces is maximized and most stable when no gaps are present between them. The success of a screwed connection is directly related to the preload reached during torque and its maintenance over time. Preload has been described as the tension generated in an abutment screw upon tightening and is a direct determinant of the clamping force. Misfit at the interface may lead to mechanical failures such as early loss of preload

and screw loosening, abutment screw fracture, implant fracture and even prosthesis fracture and potentiate clinical implant failure.^{9,49}

This misfit also results in increased microleakage,²³ gingivitis and bone loss.^{20,39} It allows micro-organisms to penetrate and colonize even into the inner part of the implant,¹⁶ leading to periodontitis, progressive bone loss approximately 2mm apical to the microgap²⁰ and eventually implant loss.^{16,47} Bacterial penetration also occurs under masticatory cycles.⁴⁶ Micro movements of the implant components during function may allow the initiation of a pumping effect, causing bacteria to move through the implant-abutment interface.³⁸ The microgap can be further enlarged under loading when the implant assembly components are subjected to eccentric forces. Thus bacterial colonization is impacted by multifactorial conditions like the precision fit between the implant components, torque forces when the components are connected and loading forces when the implants are in function.⁴⁷

The geometry of the implant-abutment connection may also affect stresses generated from loading and these stresses may have a role in development of complications.³ Implant-abutment connection geometry can be broadly classified as either external or internal connection.⁷ Currently, the internal implant-abutment connection geometry is advocated as it could potentially reduce stresses within the connection when off center loads are applied,³ and provides a strong, stable interface.^{7,49}

Commercially, pre-machined abutments are available in titanium alloy, noble metal alloys, base metal alloys, aluminium oxide alloys, zirconia and zirconia with titanium alloy connections.⁷ In order to address angulation and esthetic concerns, castable, plastic burnout patterns popularized by the UCLA abutment, that can be cast using various alloys are available.^{8,32} This burnout pattern, fits directly on top of either the implant intra-orally or on the laboratory implant analogues, which are placed in the master cast. The plastic pattern is used to develop the wax pattern for the final restoration, which will connect directly to the implant restoration.³² These UCLA type castable abutments can be cast with both noble metal alloys and base metal alloys.^{13,25,26,43} Noble metal alloys were the first to be used as castable material but with the development of economical materials for casting with significantly better mechanical properties, their use has decreased.¹⁹ Titanium alloys have exceptional mechanical properties and excellent biocompatibility. They provide excellent corrosion resistance to saline or acidic environments. Nevertheless, casting titanium alloys have a high production cost and are highly technique sensitive.⁴³ Other base metal alloys like Nickel-Chromium (Ni-Cr) and Cobalt-Chromium (Co-Cr) used in screw-retained implant supported restorations have comparable mechanical properties to that of titanium, with their modulus of elasticity being the best among all alloys used for cast restorations.^{5,26} These alloys also provide a low cost solution for screw-retained prosthesis,¹⁹ thereby reducing overall treatment costs and making it an affordable treatment option for many patients.

Fatigue test or cyclic loading tests are intended to simulate components in function, which permits analysis of possible interaction between microgap and loading.^{8,11,15,23,25,26,49} Researchers have tested the effect of cyclic loading on different aspects such as screw loosening (detorque),^{9,15,28} microgap at the interface,^{8,11,25,26,49} surface changes on implant platform or screw channel⁴⁹ and microbiological assessments.^{33,38} Cyclic loading tests evaluating the microgap have focused on various comparisons, such as, between internal and external hex connections,^{9,28} and/or between prefabricated and cast abutments¹³ and within different abutment screws,¹⁸ but with varying results. The microgap of premachined titanium abutments and cast abutments to the implant interface in single-tooth implant situations has been well documented in terms of precision of fit.^{8,13,25} Within these reports, the microgap at implant-abutment interface in castable abutments with various alloys has been shown to be greater when compared to prefabricated titanium abutments.⁸ This has been attributed to possible irregularities in the casting procedure.^{25,26} Most of these reports are based on studies using noble alloys,¹⁵ titanium alloys⁴ and few with base metal alloys.^{25,26} However, a majority of these reports have commented only on the existing or the as-cast microgap.^{8,11,25,26,49} Comparative literature on the effect of cyclic loading, on the implant-cast abutment interface (microgap) of screw-retained implant supported restoration using Ni-Cr and Co-Cr alloys in an anterior single-tooth partially edentulous situation is inadequately documented.¹³

The various techniques employed for measurement of microgap at the implant-abutment interface, include scanning electron microscopy (S.E.M.),^{12,14,53} scanning laser microscopy (S.L.M.),⁵⁰ optical microscopy,^{5,13} reflex microscopy, travelling microscopy, stereomicroscopy,²⁷ liquid strain gauges,²¹ gas permeability,⁴⁸ radiography,^{40,44} 3D micro-tomographic technique,³⁴ laser videography and photogrammetric techniques.¹¹ Scanning electron microscopy is a well-documented, precise and accurate means of measuring the microgap at the implant-abutment interface.^{8,12,14,53}

In light of the above, the aim of the present in-vitro study was to comparatively evaluate the effect of cyclic load on the microgap at the implant-abutment interface, with the cast abutment-restorations fabricated using two different base metal alloys for screw-retained implant supported restorations. The microgap measurements were done by scanning electron microscopy.

The objectives of the present study included the following:

1. To measure the microgap at the implant-abutment interface of cast abutment-restorations fabricated using Ni-Cr alloy before cyclic loading using scanning electron microscope.
2. To measure the microgap at the implant-abutment interface of cast abutment-restorations fabricated using Ni-Cr alloy after cyclic loading using scanning electron microscope.

3. To measure the microgap at the implant-abutment interface of cast abutment-restorations fabricated using Co-Cr alloy before cyclic loading using scanning electron microscope.
4. To measure the microgap at the implant-abutment interface of cast abutment-restorations fabricated using Co-Cr alloy after cyclic loading using scanning electron microscope.
5. To compare the microgap at the implant-abutment interface of cast abutment-restorations fabricated using Ni-Cr alloy before and after cyclic loading.
6. To compare the microgap at the implant-abutment interface of cast abutment-restorations fabricated using Co-Cr alloy before and after cyclic loading.
7. To compare the microgap at the implant-abutment interface of cast abutment-restorations fabricated using Ni-Cr and Co-Cr alloys before cyclic loading.
8. To compare the microgap at the implant-abutment interface of cast abutment-restorations fabricated using Ni-Cr and Co-Cr alloys after cyclic loading.
9. To compare the microgap at the implant-abutment interface of cast abutment-restorations fabricated using Ni-Cr and Co-Cr alloys both before and after cyclic loading (within and between groups).

REVIEW OF LITERATURE

Lewis SG et al (1992)³² reported on various uses of the UCLA abutment, its advantages and disadvantages when compared to conventional implant abutment. They concluded that, UCLA abutment can be used in situations to solve problems involving limited interocclusal distance, esthetics, angulation, interproximal distance between implants and soft tissue health. They also indicated a 95.8% success rate over a four year period for UCLA abutments.

Dellow AG et al (1997)¹⁴ conducted a study using scanning electron microscope (S.E.M.) to investigate the implant-abutment interface fit of four implant systems, as well as the implant-abutment fit when interchanged among the four systems. They concluded that no significant differences in microgap values were found when interchanging components. Microgap measurements were small between implant and abutment when interchanging components, indicating good machining tolerances.

Jansen VK et al (1997)²³ studied the microbial leakage at the implant-abutment interface of 13 different implant-abutment combinations. Penetration of *E.Coli* was observed for 14 days. The marginal fit at implant-abutment interface was also observed under scanning electron microscopy at x775 magnification at 4-12 locations, at right angle to the interface. In most cases, microbial leakage is observed within the first 2 days itself. Marginal gaps of

all prefabricated parts were smaller than 10 µm. It was concluded that current implant systems cannot prevent microbial leakage and bacterial colonization of the inner part of the implant.

Byrne D et al (1998)⁸ assessed the adaptation of premachined, cast, and laboratory modified premachined abutments to implants at two sites: implant-abutment interface and screw to screw seat. The samples were mounted parallel to the table of the measuring microscope to measure at two areas for fit and internal adaptation at x100 magnification. The results of this study confirmed the suggestion that premachined abutments, which include those abutments that are modified in a laboratory, are superior in adaptation to those cast from burnout patterns.

Keith SE et al (1999)²⁷ quantified the marginal discrepancy of the implant-to-prosthetic-crown interface on non-submerged dental implants restored with either a cemented or a screw-retained approach. They concluded that the mean marginal discrepancy of screw-retained metal-ceramic crowns on implant abutments is significantly smaller than that of cemented metal-ceramic crowns.

Gross M et al (1999)¹⁶ investigated the degree of microleakage at the implant-abutment interface of 5 implant systems at varying closing torque. As closing torque is increased from 10 Ncm to 20 Ncm to manufactures'

recommended closing torques, microleakage decreased significantly ($p < 0.005$) for all systems.

Cibirka RM et al (2001)⁹ examined potential differences in detorque values of abutment screws after fatigue testing with internal or external hexagon connection. Connections tested were the standard external hexagon, modified external hexagon and circular platform geometry. A fatigue testing device delivered dynamic loading forces between 20 and 200 N for 5,000,000 cycles simulating 5 years of in vivo mastication. No abutment looseness or longitudinal displacement was noted. It was concluded that increasing the vertical height, or degree of fit tolerance, between the implant external hexagon and the abutment internal hexagon or completely eliminating the implant external hexagon did not produce a significant effect on detorque values. External hexagon design only aids in surgical placement and orientation of the abutment to the implant. It does not influence force distribution or rotational resistance and may therefore affect the attainment of optimum preload during initial abutment screw tightening.

Gratton DG et al (2001)¹⁵ investigated dental implant screw joint micromotion and dynamic fatigue as a function of varied preload torque applied to abutment screws when tested under simulated clinical loading. They observed that the 16 Ncm group exhibited greater micromotion ($p < 0.001$) than both the 32 and 48 Ncm groups at all cycle intervals (2-way ANOVA, Tukey HSD). Micromotion of the implant-abutment interface remained

constant ($p = 0.99$) for each of the preload groups through 1,00,000 cycles. Under the loading parameters of this study, no measurable fatigue of the implant-abutment interface occurred. However, dental implant screw joints tightened to lower preload values exhibited significantly greater micromotion at the implant-abutment interface.

Hoyer SA et al (2001)²¹ investigated the fatigue life of UCLA-style abutment screws in wide-diameter versus conventionally sized dental implant restorations. They found that the dental implant-abutment interface of 3.75 mm and 6.0 mm externally hexed implants experienced similar joint opening after periods of dynamic loading. Laboratory adjustment of the interface significantly decreased the service life of the abutment screw joint.

Hecker DM et al (2003)¹⁸ investigated the change in fit of implant-supported prosthesis after cyclic loading and also determined the amount of change. A cyclical load of 200 N was applied for 2,00,000 cycles. They concluded that the gap dimension between the prosthetic superstructure and implant-supported abutment decreased. There was a significant ($p = 0.024$) decrease in gap dimensions when the load was applied on the anterior of the framework.

Kano SC et al (2006)²⁴ compared the loss of applied torque values between machined titanium abutments and cast UCLA-type abutments for external hex implant-abutment interface. Four groups of 12 samples each were

evaluated: (1) machined titanium abutments, (2) premachined palladium abutments cast with palladium, (3) plastic abutments cast with nickel-chromium, and (4) plastic abutments cast with cobalt-chromium. Each abutment was torqued to 30 Ncm and detorqued three times. Machined abutments demonstrated significantly greater detorque values compared with cast abutments ($p < 0.05$). No significant differences were found among cast groups. Casting procedures decrease the percentage of applied torque, which may influence the final screw joint stability.

Coelho AL et al (2007)¹¹ developed a technique to evaluate the implant-abutment gap of an external hexagon implant system as a function of radius. Implant-abutment gap distances were recorded along the implant-abutment region for each section. Individual measurements were related to their radial position through trigonometric inferences. All implants presented communication between external and internal regions through connection gaps and inaccurate implant-abutment alignment. Polynomial lines showed implant-abutment gap values below 10 μm , between 0 μm to approximately 250 μm of the implant-abutment engagement region. Gap distances significantly increased to approximately 250 μm at the outer radius of the implant-abutment engagement region.

Jaime AP et al (2007)²² evaluated the effect of cast rectifiers on the misfit of cast UCLA abutments compared to premachined UCLA abutments. The influence of casting and porcelain baking on the marginal misfit of these

components was also investigated. They concluded that the use of rectifiers in cast UCLA abutments reduced significantly, the marginal misfit at the implant-abutment interface. Even with carefully performed laboratory steps, changes at implant-abutment interface of premachined UCLA abutments occurred. Porcelain baking did not alter the marginal misfit values of UCLA abutments.

Kano SC et al (2007)²⁵ conducted a study to propose a classification system based on the horizontal and vertical microgap of the implant-abutment interface. They classified microgap as (1) ideal relationship, (2) horizontal discrepancy only, (3) vertical discrepancy only and (4) both horizontal and vertical discrepancy. Premachined cast-on abutments had significantly higher horizontal misfit than cast Ni-Cr abutments ($p < 0.001$). In the proposed classification system, 23% of all sites measured at the implant-abutment interface had an ideal relationship, 34% had a horizontal discrepancy only, 4% had a vertical discrepancy only, and 39% had both vertical and horizontal discrepancies. They concluded that the proposed implant-abutment classification system demonstrated a way to characterize and compare the microgap at the implant-abutment interface.

Roach M (2007)⁴³ reviewed the base metal alloys used for dental restorations in implants and concluded that Ni-Cr alloys have superior properties for use in porcelain-fused-to-ceramic (PFM) applications. Also their coefficient of thermal expansion is closer to that of the porcelain veneers,

which prevents cracking of the restoration. He also observed that the Co-Cr alloys are more corrosion-resistant than the Ni-Cr alloys and have physical properties similar to that of the Ni-Cr alloys, However, the coefficient of thermal expansion of Co-Cr alloys is not as compatible to that of the porcelains as the Ni-Cr alloys. Cast Titanium alloys have physical properties which is comparable to that of other base metal alloys. Also titanium alloys have excellent biocompatibility and are corrosion resistant.

Tsuge T et al (2008)⁵⁰ aimed to compare and evaluate the marginal fit and the size of microgap at the implant-abutment interface for several external and internal anti-rotation configurations. The marginal fit between implant and abutment was observed at four locations (rotating in 90° increments) under scanning electron microscope at x700 magnification. Thereafter the microgap values were determined using a scanning laser microscope at x500 magnification. They determined the microgap values of all implant-abutment interfaces examined in the study ranging from 2.3 to 5.6 µm.

Barbosa GAS et al (2008)⁴ investigated whether there is a direct correlation between the level of vertical misfit at the implant-abutment interface and torque losses in abutment screws. They concluded that there was no significant correlation between the values of vertical misfit at the implant-abutment interface and the values of torque losses applied over the UCLA abutment screws. These findings indicate that great vertical misfits do not necessarily imply higher detorque values.

Steinebrunner L et al (2008)⁴⁶ evaluated the influence of long-term dynamic loading on the fracture strength of different implant-abutment connections. Six implant systems were tested: two systems with external connections and four systems with internal connections. Fracture strength was tested with and without dynamic loading. Dynamic loading was performed in a two-axis chewing simulator with 12,00,000 load cycles at 120 N. They concluded that implant systems with long internal tube-in-tube connections and cam-slot fixation showed advantages with regard to longevity and fracture strength compared with systems with shorter internal or external connection designs.

Yüzügüllü B et al (2008)⁵³ assessed the changes in implant-abutment interface of titanium, alumina and zirconia abutments placed on Branemark implants subjected to a standard dynamic loading regimen and evaluated by scanning electron microscopy analysis. They found that after dynamic loading, there was no significant difference between aluminum oxide, zirconium oxide, and titanium abutment groups regarding the microgap at the implant-abutment interface. They also determined a decrease in the microgap values after loading for 47,250 cycles simulating 45 days of mastication in zirconia and alumina abutments. They hypothesized this decrease to fretting, resulting in loss of surface irregularities at the interface, thereby, resulting in the decrease in the marginal gap.

Tesmer M et al (2009)⁴⁷ aimed to use an in vitro model to assess the potential risk for invasion of oral microorganisms into the implant-abutment microgap of dental implants with different characteristics of the connection between the fixture and abutment. Thirty implants were divided into three groups (n = 10 per group) based on their microgap dynamics. Groups 1 and 2 were comprised of fixtures with internal Morse-taper connections that connected to standard abutments and the same abutments with a 0.5 mm groove modification, respectively. Group 3 was comprised of implants with a tri-channel internal connection. They concluded that differences in implant designs may affect the potential risk for invasion of oral microorganisms into the implant-abutment microgap.

Tsuge T et al (2009)⁴⁹ evaluated the effect of eccentric cyclic loading on abutment screw loosening in internal and external hexagon implants with either of two screw materials, titanium or gold alloy. The reverse torque value of the abutment screw was measured before (initial preload) and after loading (post-loading). In all the groups, post-loading preload was significantly higher than initial preload. They concluded that the implant-abutment connection did not have an effect on screw loosening, but the abutment screw material did. In particular, Ti abutment screws were less likely to come loose.

Cunha TDMAD et al (2010)¹² compared the vertical gap of zirconia abutment associated with implants from the same manufacturer (Procera manufacturer) and two other implant systems. They concluded that

the association of Procera zirconia abutment with other implant systems different from its manufacturer demonstrated significant alteration of vertical misfit at implant-abutment interface.

Hedge C et al (2010)¹⁹ compared the various restorative materials that can be used in implant restorations. They concluded that the use of base metal alloys in implant restorations has not been popular due to potential for corrosion between dissimilar materials. They also stated that base metal alloys have excellent physical properties and better castability when used for metal-ceramic restorations when compared to noble metal alloys. Co-Cr alloys are the most common alternative to patients allergic to nickel.

Rack A et al (2010)⁴⁰ investigated the micro-gap formation at the implant–abutment interface of two-piece dental implants using high-resolution radiography in combination with hard X-ray synchrotron radiation. Images were taken with the specimen under different mechanical loads of up to 100 N. They found that synchrotron-based radiography in comparison with classical laboratory radiography yields high spatial resolution in combination with high contrast even when exploiting micro-sized features in highly attenuating objects. The first illustration of a micro-gap which was previously indistinguishable by laboratory methods underlines that the complex micro-mechanical behavior of implants requires further in vitro investigations where synchrotron-based micro-imaging is one of the prerequisites.

Ricomini Filho AP et al (2010)⁴² evaluated the preload loss and bacterial penetration through the implant-abutment interface of conical and external hexagon connection systems subjected to thermal cycling and mechanical fatigue (TM). Four different implant-abutment connection systems were evaluated (n = 6): external hexagon with universal post, Morse taper with universal post, Morse taper with universal post through bolt, and locking taper with standard abutment. The bacterial penetration was assessed and the abutments were observed by scanning electron microscopy. They found that all screw-abutment systems showed significantly higher ($p < 0.05$) detorque values when subjected to TM and all conical systems presented bacterial penetration. The results show no relationship between the preload loss and the bacterial penetration.

Asvanund P et al (2011)³ compared the load transfer characteristics of a complete-arch restoration supported by 4 implants with external and internal implant-abutment connections. Loads were applied to the prostheses in three positions. Two-dimensional photoelastic models were used to simulate bone. Two types of implants were placed in the photoelastic models. Complete-arch metal frameworks were fabricated on the abutments. Artificial teeth were arranged on the framework, and the prosthesis was screwed onto the abutments. The specimens were analyzed at two levels (implant-abutment level and apical to the implant level) with three loading conditions (4-point load; 2-point anterior load; and 2-point lateral load). They concluded that

when loaded off-center, the internal-implant abutment connection produced less stress when compared with the external-implant abutment connection. Therefore, the internal-implant abutment connection could potentially reduce stresses within the connection when off-center loads are applied.

De Jesus Tavares RR et al (2011)¹³ evaluated the vertical misfit at the implant-abutment interface of premachined cast-on and premachined abutments of external and internal connections before and after cyclic loading. They concluded that premachined abutments presented better vertical misfit than premachined cast-on abutments for external hex implant connection, for both before and after cyclic loading analysis. Cyclic loading increased the vertical misfit of premachined cast-on external hex abutments and premachined octagonal internal abutments.

Lorenzoni FC et al (2011)³³ evaluated the sealing capability of external hexagon implant systems and assess the marginal fit. Two groups (n = 10 each) were employed: SIN (Sistema de Implantes National, Brazil) and Osseotite, (Biomet 3i, U.S.A.). S.E.M. analysis depicted gaps in the implant-abutment interface of both groups. Gaps in the implant-abutment interface were observed along with increased leakage at the 144 hours evaluation period.

Sharkey S et al (2011)⁴⁴ investigated the effect of gap size and the relative angle at which a radiograph was taken on the detection of component

misfit. Different types of implant connections (internal or external) and radiographic modalities (film or digital) were assessed. They observed that the relative angulation of the radiograph and the dimension of the gap were the most significant factors affecting an examiner's diagnostic ability. There were good inter-examiner reliability and neither the type of component used nor the radiographic media used influenced diagnostic ability. They suggested that, angulation of the X-ray beam relative to implant components needs to be controlled when using radiographs to detect component misfit.

Torres JH et al (2011)⁴⁸ conducted a study aimed at adapting the gas permeability technique used to assess endodontic sealing to implant-abutment connection leakage. A new nitrogen flow technique was developed for implant-abutment connection leakage measurement, adapted from a recent, sensitive, reproducible and quantitative method used to assess endodontic sealing. The results show very significant differences between various sealing and screwing conditions. The remaining flow was lower after key screwing compared to hand screwing ($p = 0.03$) and remained different from the negative test ($p = 0.0004$). The method reproducibility was very good, with a coefficient of variation of 1.29%. They concluded that the presented new gas flow method appears to be a simple and robust method to compare different implant systems. It allows successive measures without disconnecting the abutment from the implant and should in particular be used to assess the behavior of the connection before and after mechanical stress.

Meleo D et al (2012)³⁴ demonstrated the use of 3D micro-tomographic technique to determine the micro-gap measurements at the fixture-abutment connection surface. It also allows to acquire 3D images and to perform evaluations in a non-invasive and non-destructive and sufficiently magnified 3D reconstruction; reliable measurement of numeric data of the internal structure (morphology, structure and ultra-structure). They concluded that the connection geometry of the fixture-abutment complex influences the mechanical properties of an implant system.

Nascimento C et al (2012)³⁸ investigated the influence of repeated tightening of the abutment screw on leakage of *Streptococcus Mutans* along the interface between implants and pre-machined abutments. They found microorganisms on the internal surfaces of both groups. However, bacterial counts in group 2 were significantly higher than that in the control group ($p < 0.05$). These results suggest that bacterial leakage between implants and abutments occurs even under unloaded conditions and at a higher intensity when the abutment screw is tightened and loosened repeatedly.

MATERIALS AND METHODS

The present in-vitro study was conducted to comparatively evaluate the effect of cyclic load on the microgap at the implant-abutment interface, with the cast abutments fabricated using two different base metal alloys.

The following materials and equipments were used for the study:

MATERIALS EMPLOYED:

- Non-surface treated titanium dental implant, Standard platform, 3.75 X 11.50 mm (Seven, MIS Implants Technologies Ltd., Israel) (Fig.1)
- Spirit level indicators (Fig.2)
- Clear autopolymerizing acrylic resin (RR Cold Cure, DPI, India) (Fig.3)
- Direct plastic cylinder (abutment) internal hex with hex, MD CPH13 (MIS Implants Technologies Ltd., Israel) (Fig.4a)
- Titanium abutment screw (MIS Implants Technologies Ltd., Israel) (Fig.4b)
- 1.25 mm Hex driver, long (Zimmer Dental, U.S.A.) (Fig.5a)
- Calibrated torque wrench (Zimmer Dental, U.S.A.) (Fig.5b)
- Polyvinyl Siloxane (PVS) impression material – Addition type (Aquasil, Dentsply, Germany)
 - ❖ Soft putty/ Regular set (Fig.6a)
 - ❖ Light body consistency (Fig.6b)

- Auto mixing spiral (Yellow-70 mm, Adenta, USA) (Fig.6c)
- Auto mixing gun (Dispensing Gun 2, Heraeus Kulzer, Dormagen, Switzerland) (Fig.6d)
- Inlay casting wax (GC Corporation, Tokyo, Japan) (Fig.7)
- PKT instruments (Delta labs, Chennai, India) (Fig.8)
- 2.5 mm sprue wax (Bego, Germany) (Fig.9a)
- Surfactant spray (Aurofilm, Bego, Germany) (Fig.9b)
- Silicone investment ring and crucible former (Sili Ring, Delta labs, Chennai, India) (Fig.9c)
- Phosphate bonded investment (Bellasun, Bego, Germany) (Fig.9d)
- Colloidal silica (Begosol, Bego, Germany) (Fig.9e)
- Distilled water (Merck, Mumbai, India) (Fig.9f)
- Paint brush-small (Kiran series 024 point, India) (Fig.9g)
- Nickel-Chromium (Ni-Cr) alloy pellets (Bellabond plus, Bego, Germany) (Fig.10)
- Cobalt-Chromium (Co-Cr) alloy pellets (Wirobond C, Bego, Germany) (Fig.11)
- Casting crucible (Bego, Germany) (Fig.12a)
- Aluminum oxide powder, 50 μm (Korox, Bego, Germany) (Fig.12b)
- Carborundum separating discs (Dentorium, U.S.A.) (Fig.13a)
- Tungsten carbide burs (Edenta, Switzerland) (Fig.13b)
- Silicon carbide rubber points (Dentsply, Germany) (Fig.13c)

- Plastic instrument (API, Manipal, India) (Fig.14a)
- Light cure restorative composite (Filtex Z350 XT, 3M ESPE, Minnesota,U.S.A.) (Fig.14b)
- Custom-made jig (Fig.15)

EQUIPMENTS EMPLOYED:

- Dental surveyor (Saeshin Precision Ind. Co., Korea) (Fig.16)
- Vacuum power mixer (Whipmix, Kentucky, U.S.A.) (Fig.17)
- Burnout furnace (Technico, Technico laboratory products Pvt Ltd., Chennai, India) (Fig.18a)
- Induction casting machine (Fornax, Bego, Germany) (Fig.18b)
- Sandblaster (Delta labs, Chennai, India) (Fig.19)
- Alloy grinder (Demco, California, U.S.A.) (Fig.20)
- Light cure unit (Confident dental equipments Ltd. , India) (Fig.21)
- Scanning Electron Microscope S-3400N (Hitachi High Technologies Corporation, Japan) (Fig.22)
- Custom-made cyclic loading machine (Fig.23a&b)

Description of the custom-made cyclic loading machine (Fig.23a&b):

In the present study, a cyclic loading machine was custom-fabricated to simulate components in function, which permitted analysis of microgap at the implant-cast abutment interface and its possible interaction with loading. It consisted of a motor with gearbox, which when rotated, compressed a spring.

The spring applied a load, which was transmitted to the test sample. Its individual components and calibration are described below:

Specification of motor:

90 Watts, single phase 230V, Continuous rating, motor giving 1350 RPM with gear reduction box of 1:18 giving a final RPM of 75 (Swipfe Industries, Pune, India).

Specification of spring:

Spring load spring ISO 10243:2010 (Special Springs, Rosa, Italy)

Hole diameter – 16 mm, Rod diameter – 8 mm

Free length of spring – 38 mm

Spring constant – 48.5 N/mm

Specification of timer:

999 minutes timer with time memory (K-Pas, Chennai, India)

The motor was connected to an eccentric cam of 2.5 mm, which rotated on motor being turned on. The 2.5 mm eccentric cam compressed a spring to the same length as it rotated, generating a load of approximately 120 N. The spring transmitted the load to the stylus (3 mm diameter), which

transmitted a lesser load of approximately 109 N to the sample, due to loss of energy.

Calibration of custom-made cyclic loading device:

The maximum and minimum loads delivered by the custom-fabricated cyclic loading device were calibrated by a professional load calibration agency (Hi Tech Calibration Services, Chennai, India).

Calibrated Results:

Mode: Auto

Max. Load: 109.49 N, Min. Load: -6.52 N

Mode: Manual

Max. Load: 117.83 N, Min. Load: -7.97 N

Description of Scanning Electron Microscope (Fig.22):

Scanning electron microscope (S.E.M.) consists of a vacuum specimen chamber with a 5-axis fully motorized stage. The variable chamber pressure allows chargeup-free observation of any sample without special preparation techniques such as coating. It has a working distance of 10 mm and a magnification of x5 – x3,00,000. Auto focus and auto alignment mode was used to focus at the centre of the implant-cast abutment interface for each of the 4 surfaces. The image on the monitor was captured using a PC-SEM

software and then transferred to Quartz PCI software. Measurements were made using the Quartz PCI software and saved in jpeg format. The test sample was loaded onto the stage in the specimen chamber. Chamber door was closed and air evacuated. The specimen was then brought into focus and using the auto focus and auto alignment option, the centre of the sample was determined. The implant abutment interface was then observed at x500. For measuring the microgap, the outer perimeter of the implant-cast abutment interface was used, excluding the bevels in measurement. This was repeated for all four sides (A, B, C and D) and all twenty (n = 20) samples, both before and after loading. The image on the monitor was captured and saved using PC-SEM software and transferred to Quartz PCI software for measurements. The digital noise of the image was reduced and then inverted to identify the marginal gap, if any. Using measurement tools available in the Quartz PCI software, the microgap at the implant-cast abutment interface was measured. This image with measurement was saved.

Description of custom-made jig (Fig.15):

The custom-made jig consists of a platform and bolt. The test sample when placed in the jig platform is positioned at 30° angulation which can be secured in place with the help of a bolt.

METHODOLOGY:

- I. Preparation of stainless steel blocks and stabilizing plates
- II. Placement of implants in the stainless steel blocks
- III. Connection of direct plastic cylinder to implants
- IV. Fabrication of Ni-Cr and Co-Cr cast abutment-restorations
 - a. Preparation of wax patterns
 - b. Attachment of sprue to the wax patterns
 - c. Investment procedure
 - d. Burnout procedure
 - e. Casting procedure
 - f. Divesting and finishing the screw retained cast crowns
- V. Fixation of cast abutment-restorations to the implants
- VI. Closure of screw access hole
- VII. Measurement of the microgap at the implant-cast abutment interface
before cyclic loading
- VIII. Cyclic loading of the test samples
- IX. Measurement of the microgap at the implant-cast abutment interface
after cyclic loading
- X. Statistical analysis

I. Preparation of stainless steel blocks and stabilizing plates

(Fig.24a&b,25)

Twenty metal blocks of dimensions 25mm x 25mm x 18mm with a cylindrical mold space of diameter 18 mm and depth 16 mm were custom-fabricated (Fig.24a&b). Grooves were made in the internal surfaces of the cylindrical mold space to help retain the autopolymerizing acrylic resin. A pair of stabilizing plates was custom-fabricated (Fig.25) to hold the stainless steel block on the surveyor platform.

II. Placement of implants in the stainless steel blocks (Fig.26-30)

The surveying platform of a dental surveyor (Saeshin Precision Ind. Co., Korea) (Fig.16) was made parallel to the floor using spirit level indicators (Fig.26). The custom-made metal block was placed on the surveying platform with the mold space facing up and stabilized using custom-fabricated stabilizing plates (Fig.27). A non-surface treated titanium implant measuring 3.75mm X 11.50 mm (Seven, Standard platform, MIS Implants Technologies, Israel) (Fig.1) was connected to the surveying arm of the surveyor and positioned in the center of mold space of the custom-fabricated metal block such that the implant was submerged completely in the mold space except for 1 mm at the crest module (Fig.28). Autopolymerizing clear acrylic resin (Cold Cure, DPI, India) (Fig.3) was poured into the mold space (Fig.29) and the resin was

allowed to polymerize (Fig.30). This procedure was done to place all the twenty implants individually in twenty custom-made blocks.

III. Connection of direct plastic cylinder to implants (Fig.31):

Twenty direct plastic cylinders, (Standard platform, Direct plastic cylinder internal hex with hex, MD CPH13, MIS Implants Technologies, Israel) (Fig.4a) were connected to the implants placed in the stainless steel block by titanium abutment screw (MIS Implants Technologies Ltd., Israel) (Fig.4b) with the hex driver (Zimmer dental, U.S.A.) (Fig.5a). The samples were then randomly divided into 2 groups of 10 samples (n = 10) each. Group I (n = 10) was labeled N1 to N10 and Group II, (n = 10) C1 to C10. The 4 axial walls of the block were assigned as 'A', 'B', 'C' and 'D' to correspond to facial, mesial, palatal and distal surface of test sample respectively (Fig.31).

IV. Fabrication of Ni-Cr and Co-Cr cast abutment-restorations:

a) Preparation of wax patterns (Fig.32-34)

The wax patterns for all the samples were fabricated to obtain single piece cast abutment-restorations. The screw access hole of the direct plastic cylinder was filled and sealed with polyvinyl siloxane, putty consistency (Aquasil, Denstply, Germany) (Fig.32a). Wax pattern was prepared using inlay casting wax (GC Corporation, Tokyo, Japan) (Fig.7) by waxing over and around the connected plastic cylinder with PKT instruments (Delta labs, Chennai, India) (Fig.8). Wax-up was done

to resemble a maxillary central incisor pattern (Fig.32b). The cingulum of the central incisor was contoured to create a flat surface at a 30° inclination to the long axis of the tooth, so as to facilitate easy placement and stabilization of the stylus of the custom-made cyclic loading machine (Fig.33). An index (Fig.34a&b) was made of this wax-up using light body and soft putty consistencies of polyvinyl siloxane impression material (Aquasil, Denstply, Germany) (Fig.6a&b) and thereafter used to obtain standardized wax patterns for all the twenty samples.

b) Attachment of sprue to the wax patterns (Fig.35a)

Each wax pattern was individually sprued with preformed wax sprue (Bego, Germany) (Fig.9a) of 2.5 mm diameter. The wax sprue was attached to the incisal edge of the pattern and a reservoir was placed 1.5 mm away from the pattern. The pattern was directly sprued to the crucible former (Fig.35a) of the ringless casting system (Sili Ring, Delta labs, Chennai, India) (Fig.9c). Sprue was attached for all the twenty wax patterns in an identical manner.

c) Investment procedure (Fig.35b)

The twenty sprued wax patterns were invested individually using graphite free, phosphate-bonded investment material (Bellasun, Bego, Germany) (Fig.9d). A 6 mm distance was provided between the patterns and top of the ring. All patterns were sprayed with surfactant spray (Aurofilm, Bego, Germany) (Fig.9b), to aid in better wetting the wax pattern by the investment material. As per the manufacturer's

recommendations, 160 gms of the phosphate-bonded investment was mixed with 38 ml of investment liquid, which was prepared by mixing 30 ml of colloidal silica (Begosol, Bego, Germany) (Fig.9e) and 8 ml of distilled water (Fig.9f) in the ratio of 3:1. The investment powder was first hand mixed with a spatula until the entire material was wetted thoroughly followed by vacuum mixing for 30 seconds using vacuum power mixer (Whipmix, Kentucky, U.S.A.) (Fig.17). Once the investment was mixed the entire pattern was painted with a thin layer of investment using a small paintbrush (Kiran series 024 point, India) (Fig.9g). The silicon investment ring was positioned on the crucible former and the remaining investment mix was vibrated slowly in to the ring (Fig.35b). The invested patterns were allowed to bench set for 20 minutes, and the silicon investment ring was removed.

d) Burn out procedure (Fig.35c)

All the invested patterns were placed in a burnout furnace (Technico, Technico laboratory products Pvt. Ltd., Chennai, India) (Fig.18a) for pattern elimination. Investments with the patterns were left in the burnout furnace for a period of three hours (Fig.35c). During the first hour, the temperature was raised from room temperature to 380°C; in the second hour, the temperature was raised to 900°C and during the last hour the temperature was sustained at 900°C to accomplish complete burnout of the pattern without any residue. The investment mold was initially placed in the furnace such that the crucible end was in contact

with the floor of the furnace for the escape of molten material. The investment mold was reversed later near the end of burnout cycle with the sprue hole facing upward to enable escape of the entrapped gases and also to allow oxygen contact to ensure complete burnout of the wax pattern.

e) Casting procedure (Fig.35d)

Casting was accomplished for wax patterns of Group I samples, N1 to N10 with Ni-Cr alloy (Bellabond plus, Bego, Germany) (Fig.10). Similarly, the wax patterns for Group II samples, C1 to C10 were cast with Co-Cr alloy (Wirobond C, Bego, Germany) (Fig.11) The casting procedure was performed in an induction casting machine (Fornax, Bego, Germany) (Fig.18b) quickly to prevent heat loss resulting in thermal contraction of the mold for both the alloys. The Ni-Cr and Co-Cr alloy were heated sufficiently till the alloy ingot turned to molten state and the crucible (Fig.12a) was released. Separate crucibles were employed for melting Ni-Cr and Co-Cr alloys to avoid contamination. The centrifugal force ensured the complete flow of the molten metal into the mold space (Fig.35d).

f) Divesting and finishing the cast abutment-restorations (Fig.36a,b,c,d&e)

Following casting, the hot casting was allowed to return to room temperature (Fig.36a). A knife was used to trim the investment at the bottom end of the ring. It was then broken apart (Fig.36b) and the

remaining investment was slowly removed with a hammer. Adherent investment was removed from the casting by air abrading with 50 μm alumina (Korox, bego, Germany) (Fig.12b) at 80 psi pressure in a sand blasting machine (Delta labs, Chennai, India) (Fig.36c). Sprue was cut using 0.7 mm thin separating discs (Dentorium, New York, U.S.A.) (Fig.36d). The casting was inspected under magnification for casting defects. Casting with irregularities in the internal margin, distorted surfaces, were discarded. External surfaces were relieved of all nodules with a round carbide bur. The cast abutment-restoration was minimally finished using metal trimming burs (Edenta, Switzerland) and silicon white and grey carbide rubber points (Fig.13a,b&c), (Dentsply, Germany) (Fig.36e). The same procedure was repeated for all of the twenty cast abutment-restorations fabricated with Ni-Cr and Co-Cr alloys (Ni-Cr = 10; Co-Cr = 10).

V. Fixation of cast abutment-restorations to the implants (Fig.37):

Each finished cast abutment-restoration (Fig.36e) was connected to its corresponding implant placed in the stainless steel block with the respective abutment screw using a hex driver (Zimmer Dental, U.S.A.) (Fig.5a) and torqued to 35 Ncm using a calibrated torque wrench (Zimmer Dental, U.S.A.) (Fig.5b), as recommended by the manufacturer (Fig.37). The same procedure was repeated for all of the twenty cast abutment-restorations fabricated with Ni-Cr and Co-Cr alloys (Ni-Cr = 10; Co-Cr = 10).

VI. Closure of screw access hole (Fig.38a&b)

Light-cure restorative composite (Filtex Z350 XT, 3M ESPE, Minnesota, U.S.A.) (Fig.14b) was used to close the screw access hole. The screw access hole was first half filled with cotton and condensed using a plastic instrument (API, Manipal, India) (Fig.14a). Light-cure composite material was filled in layers of 2 mm into the remaining top half of the screw access hole and condensed (Fig.38a). U-V light from light cure unit (Confident dental equipments Ltd., India) (Fig.21) was shown after each layer for a period of 40 seconds at a maximum distance of 1 mm from the samples as recommended by the manufacturer (Fig.38b). This procedure was repeated to obtain a total of twenty test samples, ten (n = 10) of Group I (Ni-Cr) (Fig.39a) and ten (n = 10) of Group II (Co-Cr) (Fig.39b).

VII. Measurement of the microgap at the implant-cast abutment interface before cyclic loading (Fig.40a,b,c&d,41a&b):

Each test sample was placed on the platform of a scanning electron microscope S-3400N (Hitachi High Technologies Corporation, Japan) (Fig.22) and the microgap at the implant-cast abutment interface (Fig.40a,b,c&d) was measured at x500 zoom lens magnification (Fig.41a&b). The measurements were obtained for four surfaces namely, A - facial, B - mesial, C -palatal and D - distal, for each test sample. This was repeated for all twenty samples and recorded in micrometers (μm).

Thus, the microgap for ten ($n = 10$) samples of Group I (Ni-Cr) and ten ($n = 10$) samples of Group II (Co-Cr) was measured before cyclic loading. Mean microgap values for each test sample and then for each test group was calculated and the data was statistically analyzed.

VIII. Cyclic loading of the test samples (Fig.42a&b):

A cyclic loading test is intended to simulate components in function, thus permitting analysis of possible interaction between microgap at the implant-cast abutment interface and loading. Cyclic loading was performed individually for all twenty (Ni-Cr = 10; Co-Cr = 10) test samples to simulate oral loading conditions. The test sample was placed in a custom-made jig (Fig.15), which was positioned and secured at a 30° angle to the floor to simulate the direction of non-axial loading forces in maxillary anterior region. This jig was attached to the cyclic loading machine. The stylus was placed on the flattened cingulum portion of the central incisor (Fig.42a) and it was subjected to cyclic loading (Fig.42b). A sinusoidal waveform at 1.25 Hz for load between 0 to 109 N (approximately) simulating human masticatory frequency and loads were applied. This cycle was continued for 2000 minutes. The timer was set for 2 consecutive cycles of 999 minutes and then 1 cycle of 2 minutes, for each test sample. It simulated approximately 1,50,000 cycles or 6 months of function. Cyclic loading was performed in a dry environment. This procedure was repeated for all twenty (Ni-Cr = 10; Co-Cr = 10) test samples.

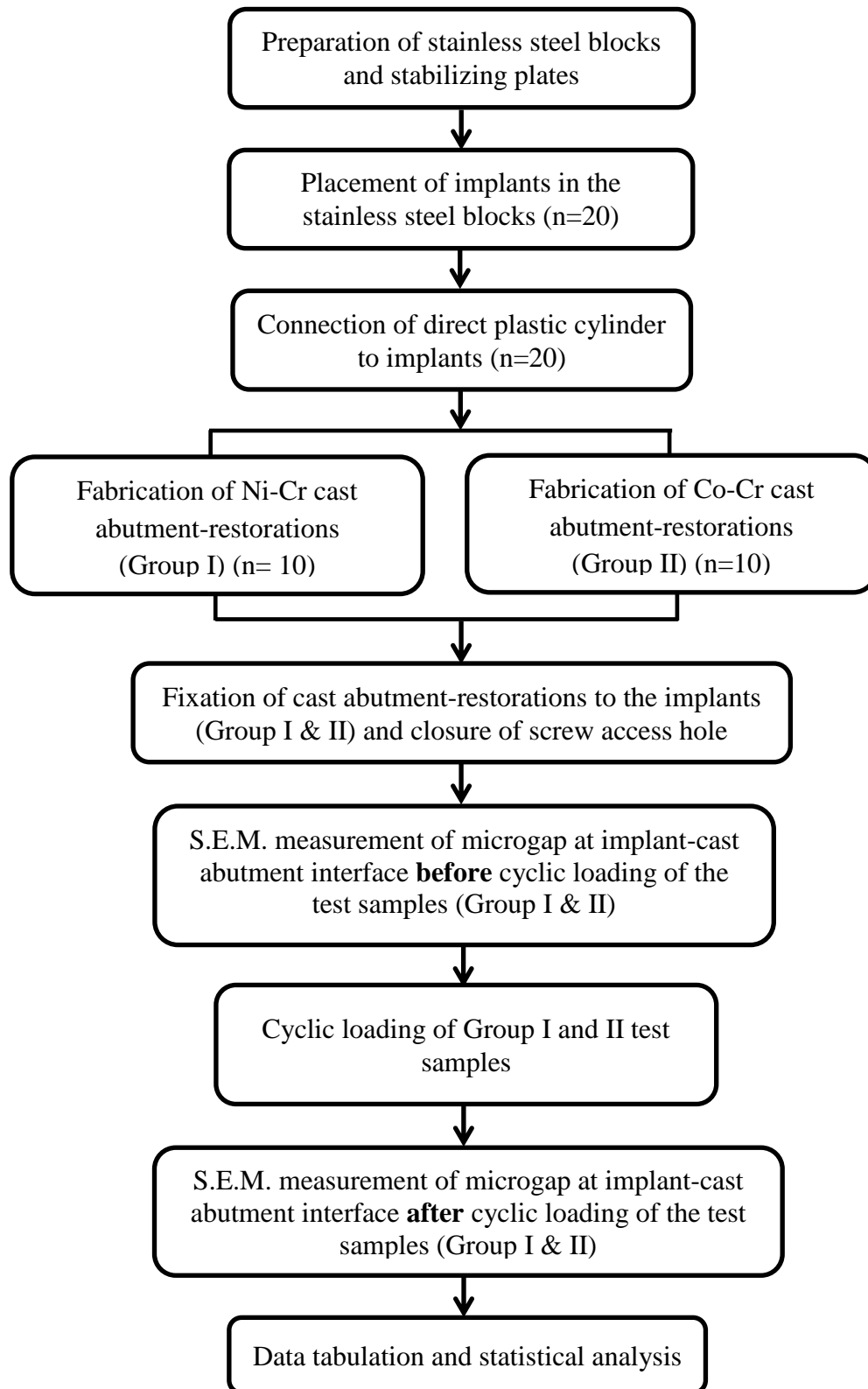
IX. Measurement of the microgap at the implant-cast abutment interface after cyclic loading (Fig.43a&b):

After cyclic loading, each test sample was individually inspected visually and tactically for deformation and/or cast abutment-restoration loosening. Each verified test samples was placed individually on the platform of the scanning electron microscope S-3400N (Hitachi High Technologies Corporation, Japan) (Fig.22) and the microgap at the implant-cast abutment interface was measured at x500 magnification (Fig.43a&b). The measurements were obtained in a manner similar to that described previously for test samples prior to cyclic loading. Thus, the microgap for ten (n = 10) samples of Group I and ten (n = 10) samples of Group II was measured after cyclic loading. Mean microgap values for each test sample and then for each test Group was calculated and the data was statistically analyzed.

X. Statistical analysis:

The tabulated results were subjected to statistical analysis. All statistical calculations were performed using Microsoft Excel 10 (Microsoft, USA) and SPSS (SPSS for Windows 10.0.5, SPSS Software Corp., Munich, Germany) software. Paired 't'-Test was used for the comparison of mean microgap values obtained before and after cyclic loading in Group I (Ni-Cr) and Group II test samples (Co-Cr) (within groups). Independent 't'- Test was then used to compare the mean microgap values obtained from Ni-Cr (Group I) and Co-Cr (Group II) test samples both before and after cyclic loading respectively (between groups).

METHODOLOGY – OVERVIEW



MATERIALS & EQUIPMENTS



**Fig.1: Non-surface treated titanium dental implant, standard platform,
3.75 x 11.50 mm**

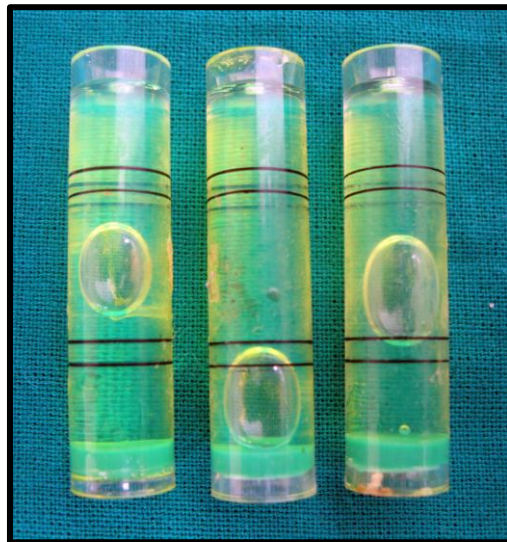


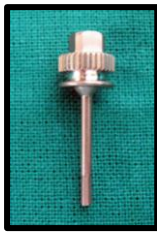
Fig.2: Spirit level indicators



Fig.3: Clear auto polymerizing acrylic resin



**Fig.4a: Direct plastic cylinder internal hex with hex
b: Titanium abutment screw**



a



b

Fig.5 a: 1.25 mm Hex drive, Long
b: Calibrated torque wrench



Fig.6a: Soft Putty, Polyvinyl Siloxane impression material-Addition type
b: Light Body, Polyvinyl Siloxane impression material-Addition type
c: Auto mixing spiral
d: Auto mixing gun



Fig.7: Inlay casting wax



Fig.8: PKT Instruments



Fig.9a: 2.5 mm sprue wax

b: Surfactant spray

c: Investment ring and crucible former

d: Phosphate bonded investment

e: Colloidal silica

f: Distilled water

g: Paint brush



Fig.10: Nickel-Chromium (Ni-Cr) alloy pellets



Fig.11: Cobalt-Chromium (Co-Cr) alloy pellets



Fig.12a: Casting crucible



Fig.12b: Al₂O₃ powder

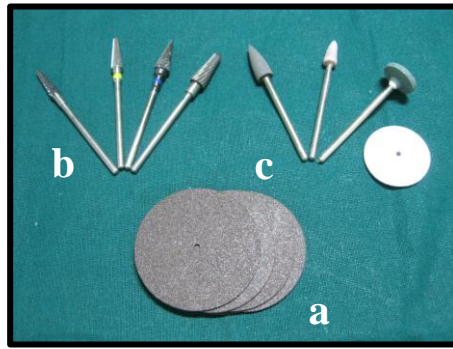


Fig. 13a: Carborundum separating discs

b: Tungsten carbide burs

c: Silicon carbide rubber points

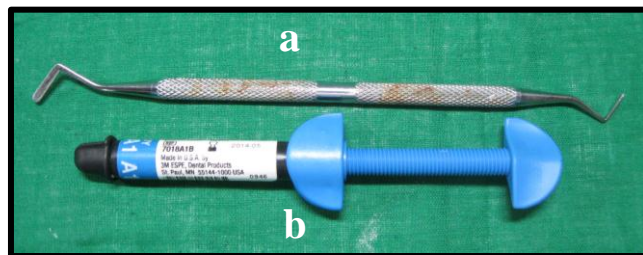


Fig.14a: Plastic instrument

b: Light cure restorative composite



Fig.15: Custom-made jig



Fig.16: Dental surveyor



Fig.17: Vacuum power mixer



Fig.18a: Burnout furnace



Fig.18b: Induction casting machine



Fig.19: Sandblaster



Fig.20: Alloy grinder



Fig.21: Light cure unit

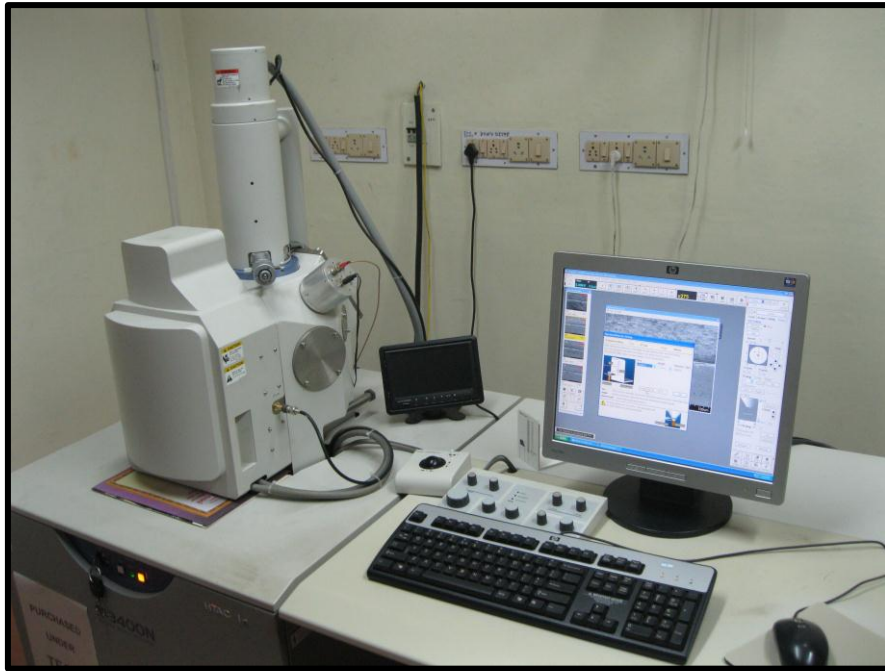


Fig.22: Scanning Electron Microscope



Fig.23a: Custom-made cyclic loading machine

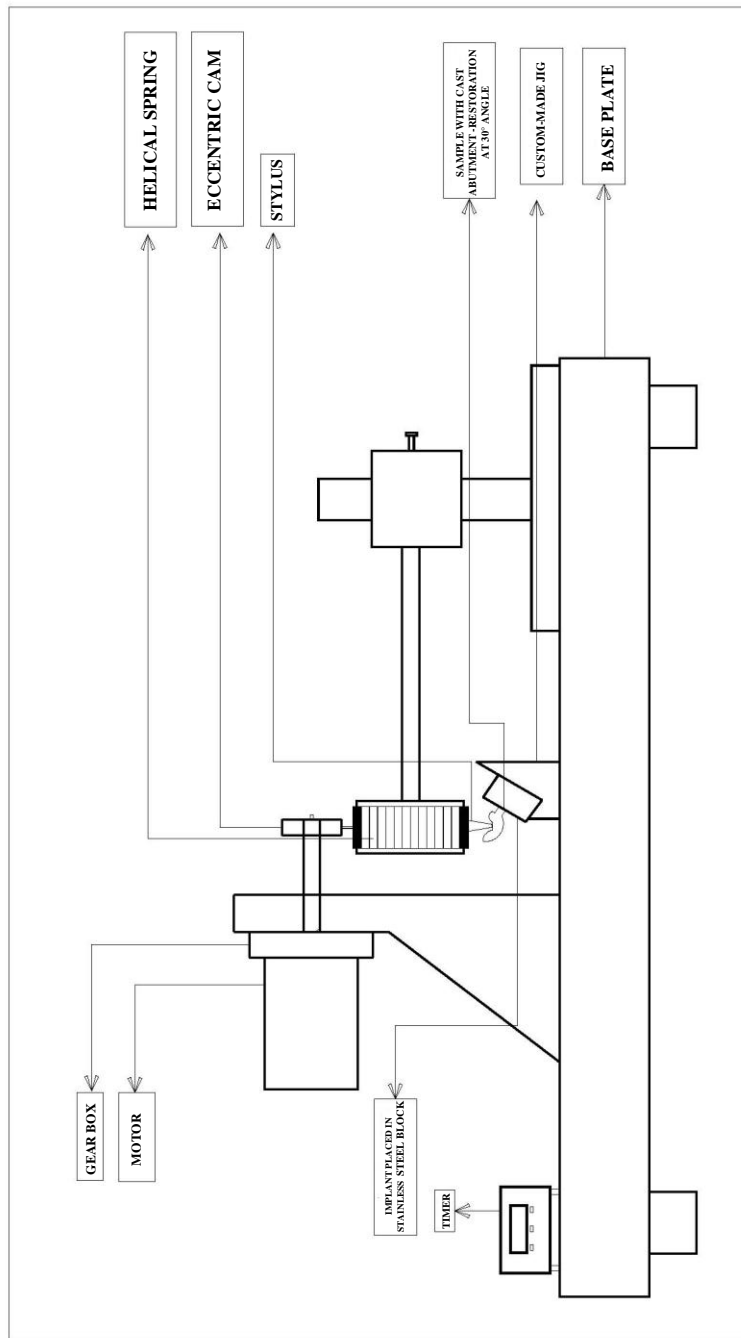


Fig.23b: Line diagram for custom-made cyclic loading machine

METHODOLOGY

PREPARATION OF STAINLESS STEEL BLOCKS AND STABILIZING PLATES

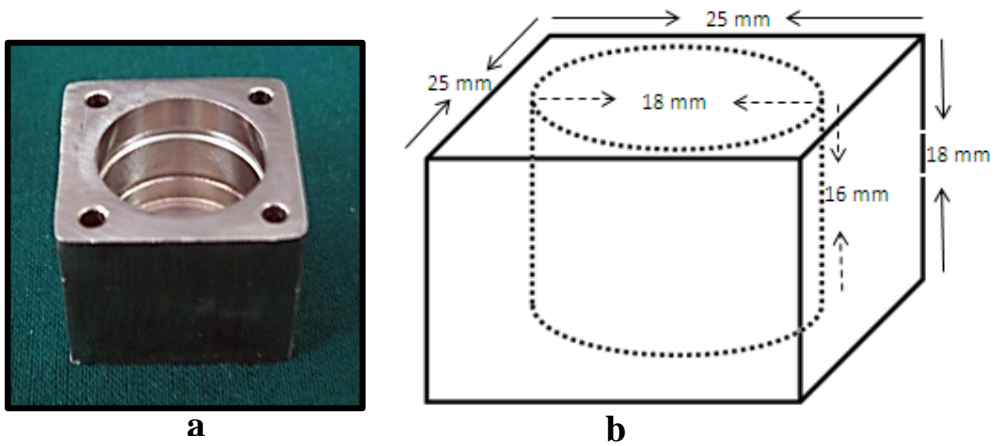


Fig.24a: Custom-made stainless steel block

b: Line diagram of custom-made stainless steel block

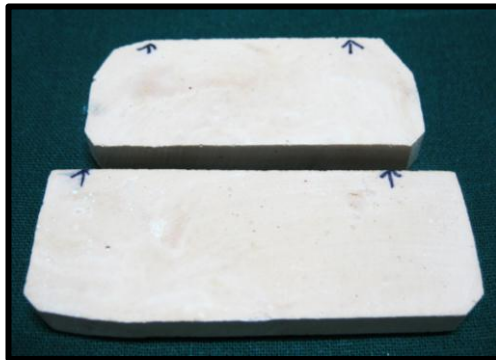


Fig.25: Custom made stabilizing plates

PLACEMENT OF IMPLANTS IN STAINLESS STEEL BLOCKS



Fig.26: Surveying platform made parallel to the floor using spirit level indicators

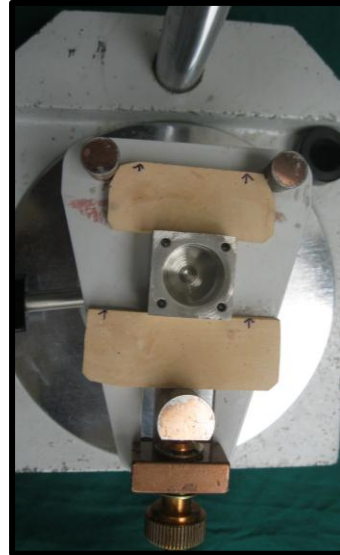


Fig.27: Stabilized stainless steel block

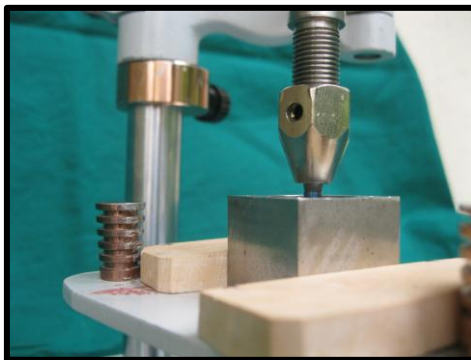


Fig.28: Non-surface treated titanium implant positioned in the stainless steel block

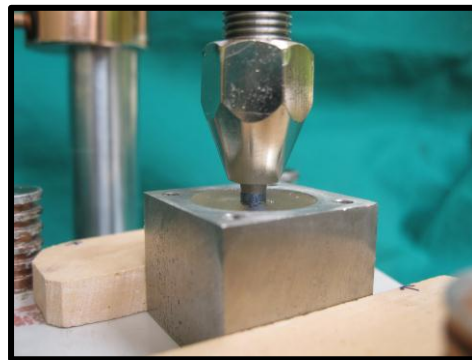


Fig.29: Autopolymerizing clear acrylic resin poured in the mold space

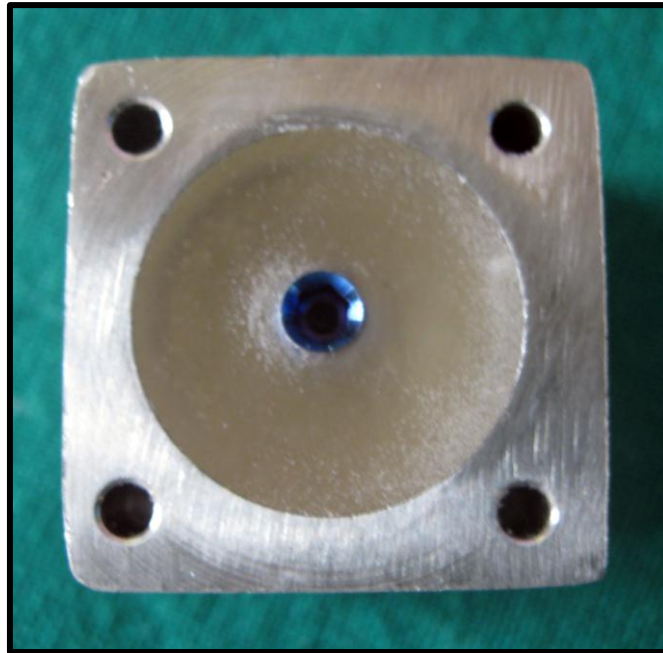


Fig.30: Implant placed in clear acrylic resin

CONNECTION OF DIRECT PLASTIC CYLINDER TO IMPLANTS

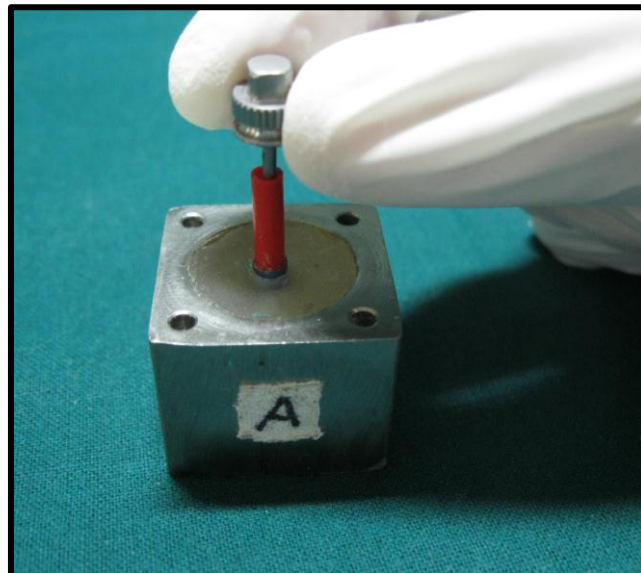


Fig.31: Connecting direct plastic cylinder to implant

FABRICATION OF Ni-Cr AND Co-Cr CASTABUTMENT-RESTORATIONS

Preparation of wax patterns

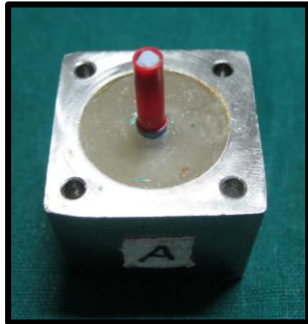


Fig.32a: Screw access hole closed with putty polyvinyl siloxane

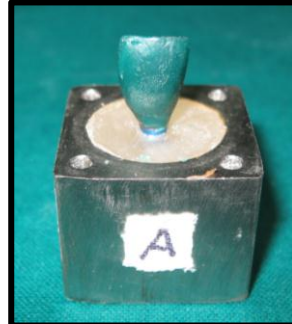


Fig.32b: Wax-up on plastic cylinder



Fig.33: Cingulum contoured to flat surface at 30° to long axis of tooth

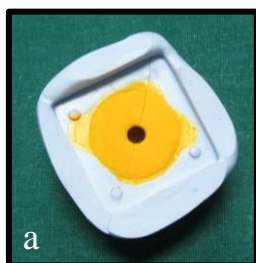


Fig.34a: Index for duplicating the wax patterns
b: Index for duplicating the wax patterns (inside view)



Fig.35a: Pattern attached to crucible former



Fig.35b: Investing the pattern



Fig.35c: Burnout procedure



Fig.35d: Casting procedure

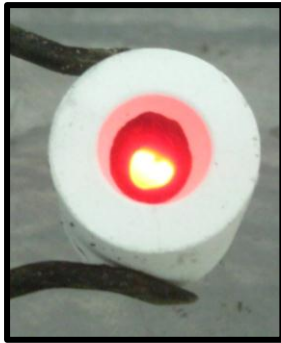


Fig.36a: Completed casting with button



Fig.36b: Partially cleaned casting



Fig.36c: Sandblasted casting



Fig.36d: Casting after sprue sectioning

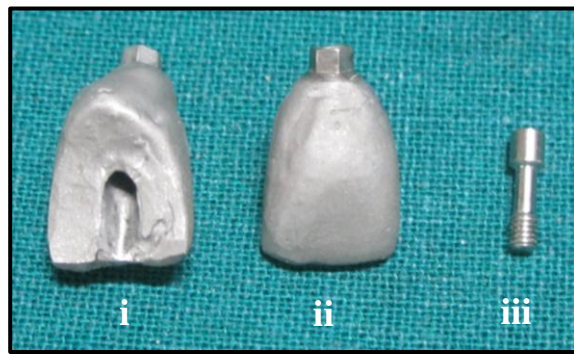


Fig.36e: Completed restoration (i & ii) and prosthetic screw (iii)

FIXATION OF CAST ABUTMENT-RESTORATION TO THE IMPLANTS

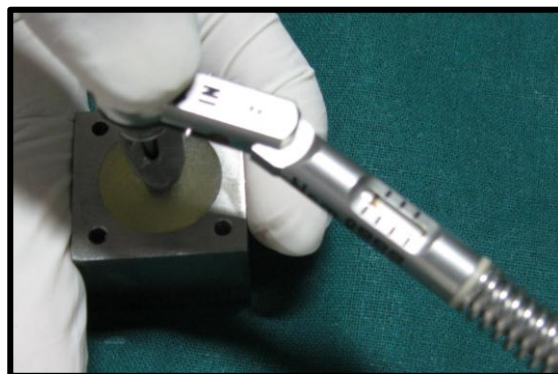


Fig.37: Fixation of cast abutment-restoration using calibrated torque wrench

CLOSURE OF SCREW ACCESS HOLE



Fig.38a: L.C. restorative composite filled into the screw access hole



Fig.38b: L.C. composite cured

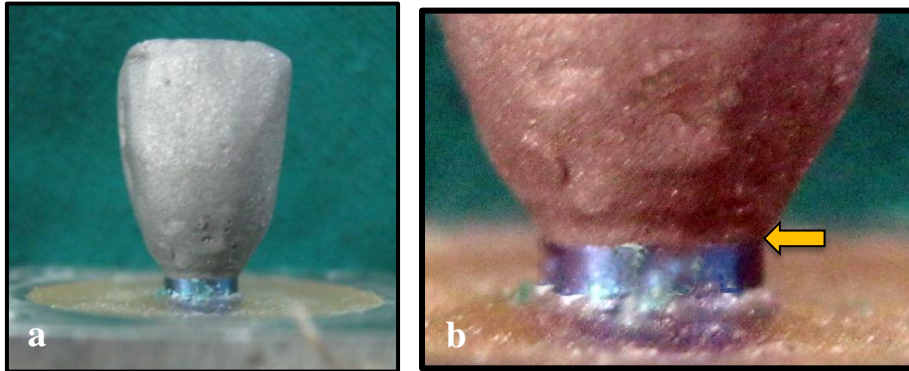


Fig.39a: Group I test samples - Ni-Cr cast abutment-restorations

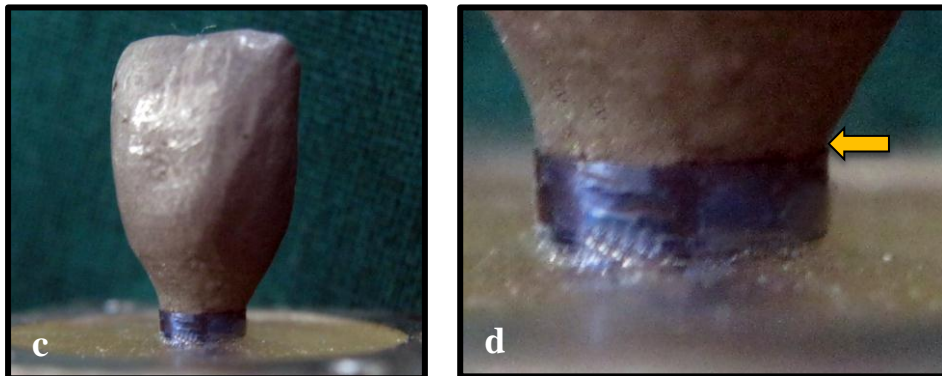


Fig.39b: Group II test samples - Co-Cr cast abutment-restorations

**MEASUREMENT OF THE MICROGAP AT THE IMPLANT-CAST
ABUTMENT INTERFACE BEFORE CYCLIC LOADING**



**Fig.40a&b: Implant-cast abutment interface (Ni-Cr)
Arrow indicates implant-cast abutment interface**



**Fig.40c&d: Implant-cast abutment interface (Co-Cr)
Arrow indicates implant-cast abutment interface**

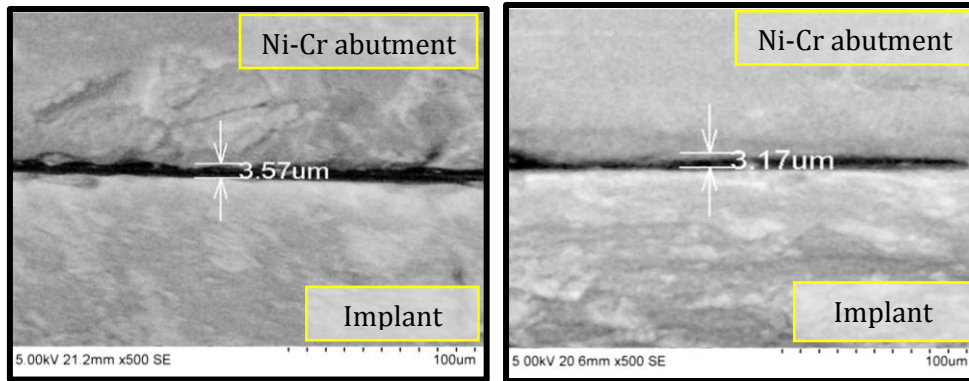


Fig.41a: Measurement of microgap at implant-cast abutment interface before cyclic loading of Group I (Ni-Cr) using Scanning Electron Microscope (S.E.M.) at x500

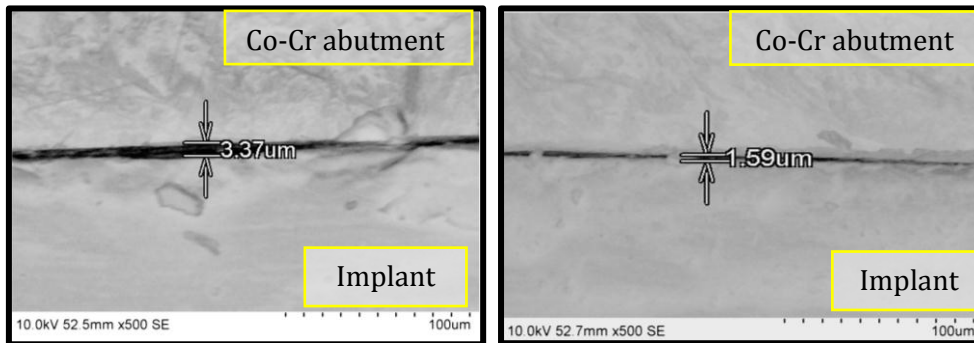


Fig.41b: Measurement of microgap at implant-cast abutment interface before cyclic loading of Group II (Co-Cr) using Scanning Electron Microscope (S.E.M.) at x500

CYCLIC LOADING OF THE TEST SAMPLES



Fig.42a: Stylus placed on flattened cingulum of test sample

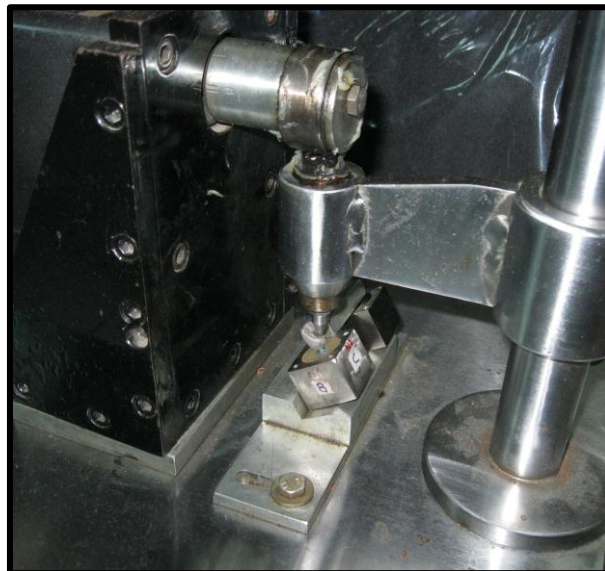


Fig.42b: Cyclic loading of the test sample

MEASUREMENT OF THE MICROGAP AT THE IMPLANT-CAST ABUTMENT INTERFACE AFTER CYCLIC LOADING

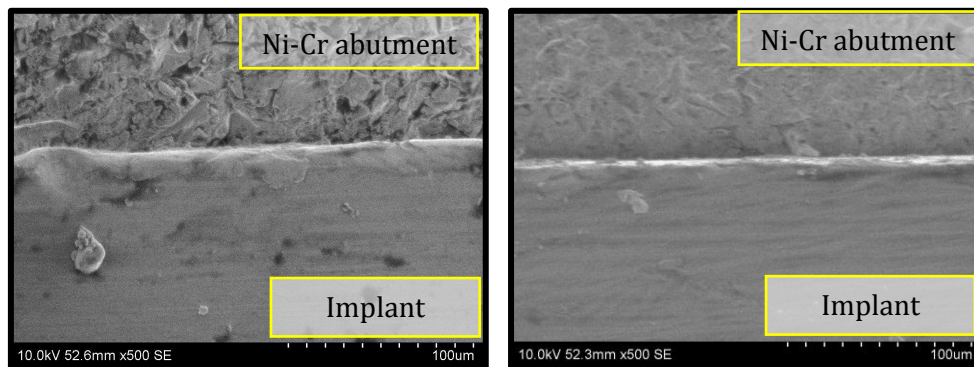


Fig.43a: Measurement of microgap at implant-cast abutment interface after cyclic loading of Group I (Ni-Cr) using Scanning Electron Microscope (S.E.M.) at x500

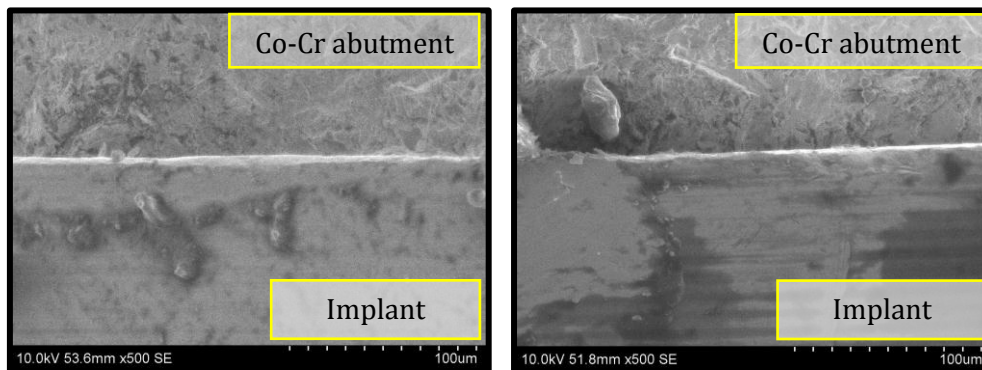


Fig.43b: Measurement of microgap at implant-cast abutment interface after cyclic loading of Group II (Co-Cr) using Scanning Electron Microscope (S.E.M.) at x500

COMPARATIVE S.E.M. PICTURES (Ni-Cr)

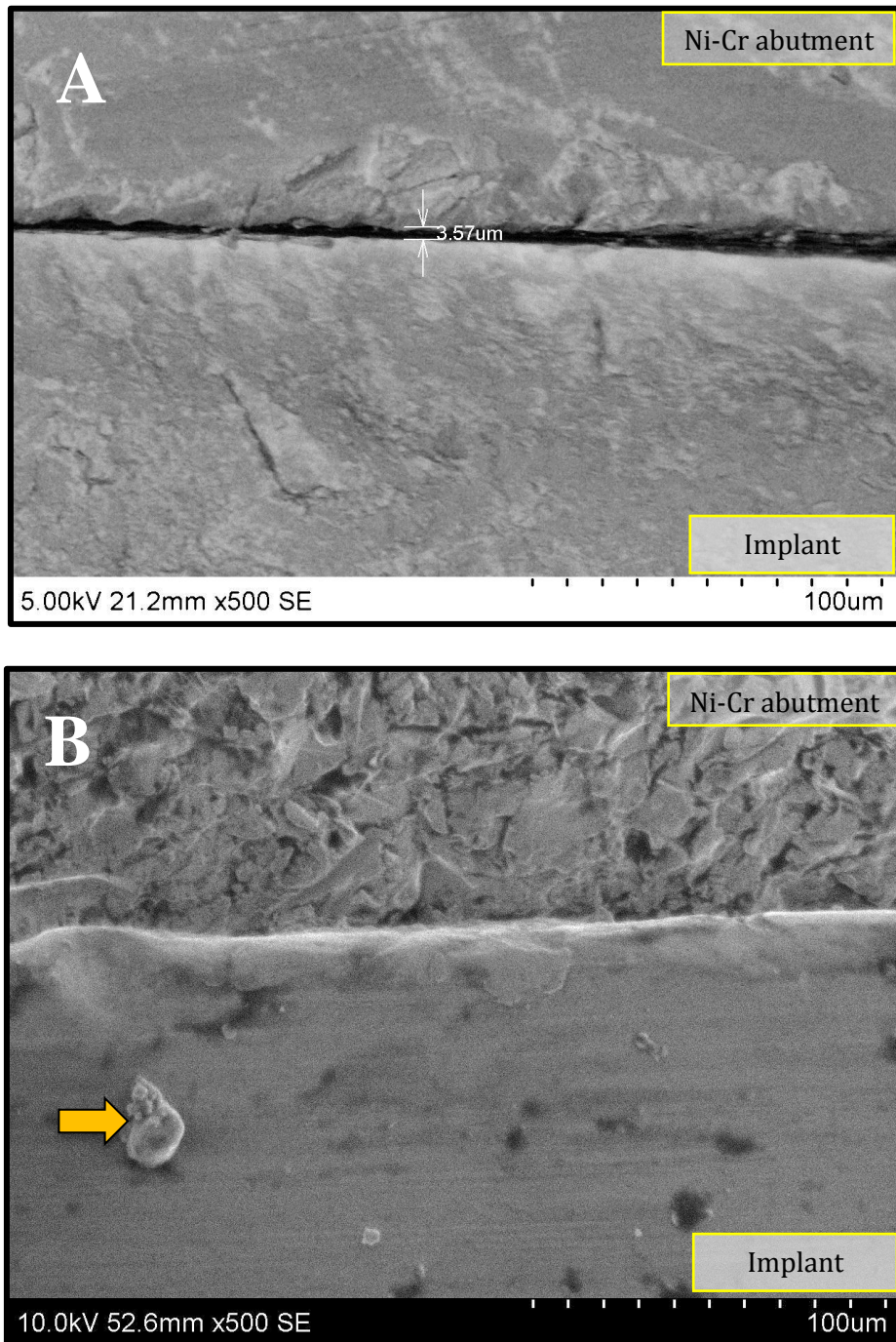


Fig.44: Decrease in microgap at implant-cast abutment interface
a) Before b) After cyclic loading of Group I (Ni-Cr) using Scanning
Electron Microscope at x500. Arrow indicates debris

COMPARATIVE S.E.M. PICTURES (Co-Cr)

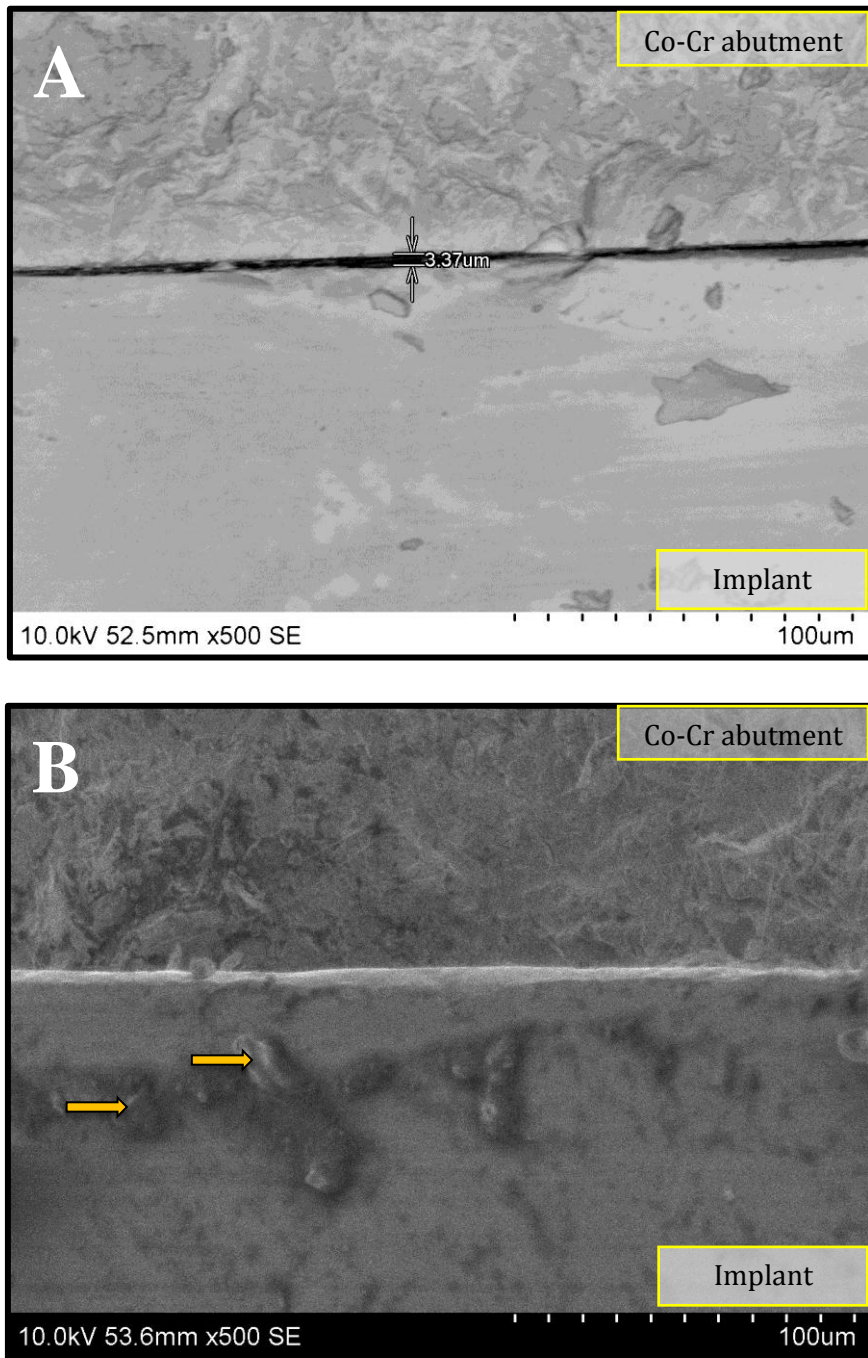


Fig.45: Decrease in microgap at implant-cast abutment interface
a) Before b) After cyclic loading of Group II (Co-Cr) using Scanning
Electron Microscope at x500. Arrow indicates debris

RESULTS

The present in-vitro study was conducted to comparatively evaluate the effect of cyclic load on the microgap at the implant-abutment interface, with the cast abutment-restorations fabricated using two different base metal alloys.

Twenty titanium implants were placed individually into autopolymerizing acrylic resin in custom-made stainless steel blocks. The embedded implants were randomly divided into two groups of ten each (Group I & Group II). In Group I, ten Ni-Cr screw-retained cast abutment-restorations and in Group II, ten Co-Cr screw-retained cast abutment-restorations were connected with a hex driver to their corresponding embedded implants in the stainless steel blocks and torqued to 35 Ncm with a torque wrench. The test samples were then labeled as N1 to N10 for Ni-Cr group and C1 to C10 for Co-Cr group. The screw access hole was closed with light cure composite restorative material. The facial, mesial, palatal and distal surfaces were labeled as A, B, C and D respectively. The microgap was measured at the implant-cast abutment interface at x500 magnification using scanning electron microscope for all twenty samples before cyclic loading. The measurements were obtained in micrometers (μm) for four surfaces (A, B, C and D), of each test sample. The test samples were then subjected to cyclic loading and the microgap was measured again at the implant-cast abutment interface at the same four surfaces for all twenty samples. The results obtained from the study were tabulated and subjected to statistical analysis.

Table I shows basic values and mean microgap at the implant-cast abutment interface of Group I samples (Ni-Cr) before cyclic loading.

Table II shows basic values and mean microgap at the implant-cast abutment interface of Group I samples (Ni-Cr) after cyclic loading.

Table III shows basic values and mean microgap at the implant-cast abutment interface of Group II samples (Co-Cr) before cyclic loading.

Table IV shows basic values and mean microgap at the implant-cast abutment interface of Group II samples (Co-Cr) after cyclic loading.

Table V shows the comparison between mean values of microgap at implant-cast abutment interface of Group I samples (Ni-Cr) before and after cyclic loading using Paired 't'-Test.

Table VI shows the comparison between mean values of microgap at implant-cast abutment interface of Group II samples (Co-Cr) before and after cyclic loading using Paired 't'-Test.

Table VII shows the comparison between mean values of microgap of Group I (Ni-Cr) and Group II (Co-Cr) samples at implant-cast abutment interface before cyclic loading using Independent 't'-Test.

Table VIII shows the comparison between mean values of microgap of Group I (Ni-Cr) and Group II (Co-Cr) samples at implant-cast abutment interface after cyclic loading using Independent 't'-Test.

Table IX shows the overall comparison between mean values of microgap at implant-cast abutment interface of Group I (Ni-Cr) and Group II (Co-Cr) samples before and after cyclic loading.

Graph I shows basic values of microgap at implant-cast abutment interface for Group I samples (Ni-Cr) before cyclic loading.

Graph II shows basic values of microgap at implant-cast abutment interface for Group I samples (Ni-Cr) after cyclic loading.

Graph III shows basic values of microgap at implant-cast abutment interface for Group II samples (Co-Cr) before cyclic loading.

Graph IV shows basic values of microgap at implant-cast abutment interface for Group II samples (Co-Cr) after cyclic loading.

Graph V shows the comparison between mean values of microgap at implant-cast abutment interface of Group I samples (Ni-Cr) before and after cyclic loading.

Graph VI shows the comparison between mean values of microgap at implant-cast abutment interface of Group II samples (Co-Cr) before and after cyclic loading.

Graph VII shows the comparison between mean values of microgap of Group I (Ni-Cr) and Group II (Co-Cr) samples at implant-cast abutment interface before cyclic loading.

Graph VIII shows the comparison between mean values of microgap of Group I (Ni-Cr) and Group II (Co-Cr) samples at implant-cast abutment interface after cyclic loading.

Graph IX shows the overall comparison between mean values of microgap at implant-cast abutment interface of Group I (Ni-Cr) and Group II (Co-Cr) samples before and after cyclic loading.

Table I: Basic values and mean microgap at the implant-cast abutment interface of Group I samples (Ni-Cr) before cyclic loading

Sample No.	Microgap (μm)				Sample Mean (μm)
	Surface A	Surface B	Surface C	Surface D	
N1	3.57	3.17	3.77	4.37	3.72
N2	4.38	2.78	0.992	2.78	2.733
N3	1.59	3.97	6.35	2.39	3.575
N4	3.4	2.39	1.59	1.98	2.34
N5	1.59	1.6	1.79	1.59	1.6425
N6	3.92	1.58	1.22	3.02	2.435
N7	1.85	3.54	3.7	1.98	2.7675
N8	3.94	3.35	5.38	3.64	4.0775
N9	2.22	3.06	2.27	1.13	2.17
N10	2.63	2.43	0.974	3.88	2.4785
Group Mean					2.7939

Maximum microgap – 6.35 μm

Minimum microgap – 0.974 μm

Mean microgap – 2.7939 μm

Table II: Basic values and mean microgap at the implant-cast abutment interface of Group I samples (Ni-Cr) after cyclic loading

Sample No.	Microgap (μm)				Sample Mean (μm)
	Surface A	Surface B	Surface C	Surface D	
N1	1.99	1.39	0	0.794	1.0435
N2	0	0	0	0	0
N3	0	0	0	0	0
N4	0	0	0	0	0
N5	0	0	0	0	0
N6	0	0	0	0	0
N7	0	1.84	0	0	0.46
N8	0	0	0	0	0
N9	0	0	0	1.64	0.41
N10	0	0	0	0	0
Group Mean					0.1914

Maximum microgap – 1.99 μm

Minimum microgap – 0.00 μm

Mean microgap – 0.1914 μm

Table III: Basic values and mean microgap at the implant-cast abutment interface of Group II samples (Co-Cr) before cyclic loading

Sample No.	Microgap (μm)				Sample Mean (μm)
	Surface A	Surface B	Surface C	Surface D	
C1	0.992	2.58	2.38	1.79	1.9355
C2	1.59	1.99	1.19	2.18	1.7375
C3	1.39	0.595	11.1	6.95	5.0087
C4	2.38	12.7	3.37	2.58	5.2575
C5	3.37	1.59	0.992	1.59	1.8855
C6	2.1	1.5	1.6	2.04	1.81
C7	2.61	1.02	1.18	2.36	1.7925
C8	1.15	2.22	1.02	1.1	1.3725
C9	1.83	1.34	1.23	2.72	1.78
C10	1.47	1.55	0.749	1.92	1.4222
Group Mean					2.4002

Maximum microgap – 12.7 μm

Minimum microgap – 0.595 μm

Mean microgap – 2.4002 μm

Table IV: Basic values and mean microgap at the implant-cast abutment interface of Group II samples (Co-Cr) after cyclic loading

Sample No.	Microgap (μm)				Sample Mean (μm)
	Surface A	Surface B	Surface C	Surface D	
C1	0	0	0	0	0
C2	0	0	0	0	0
C3	0	0	0	4.77	1.1925
C4	0	0	0	0	0
C5	0	0	0	0	0
C6	0	0	0	0	0
C7	0	0	0	0	0
C8	0	6.32	0	0	1.58
C9	0	0	0	0	0
C10	0	0	0	0	0
Group Mean					0.2773

Maximum microgap – 6.32 μm

Minimum microgap – 0.00 μm

Mean microgap – 0.2773 μm

Table V: Comparison between mean values of microgap at implant-cast abutment interface of Group I samples (Ni-Cr) before and after cyclic loading using Paired ‘t’-Test

GROUP I (Ni-Cr)	No. of samples	Mean Microgap (µm)	Mean microgap difference (µm)	Standard Deviation	p - value
Before cyclic loading	10	2.7939	2.6025	0.7434	.000*
After cyclic loading	10	0.1914			

*p - value < 0.05; significant at 5% level

Inference:

On statistical analysis using Paired ‘t’-Test to compare the mean microgap at the implant-cast abutment interface of cast abutment-restorations fabricated using Ni-Cr (Group I) before and after cyclic loading, it was found that the mean microgap of Group I samples after cyclic loading was lower than the mean microgap before cyclic loading and the difference was statistically significant (p - value was < 0.05).

Table VI: Comparison between mean values of microgap at implant-cast abutment interface of Group II samples (Co-Cr) before and after cyclic loading using Paired ‘t’-Test

GROUP II (Co-Cr)	No. of samples	Mean Microgap (µm)	Mean microgap difference (µm)	Standard Deviation	p - value
Before cyclic loading	10	2.4002	2.1229	1.45981	.001*
After cyclic loading	10	0.2773			

* p - value < 0.05; significant at 5% level

Inference:

On statistical analysis using Paired ‘t’-Test to compare the mean microgap at the implant-cast abutment interface of cast abutment-restorations fabricated using Co-Cr (Group II) before and after cyclic loading, it was found that the mean microgap of Group II samples after cyclic loading was lower than the mean microgap before cyclic loading and the difference was statistically significant (p - value was < 0.05).

Table VII: Comparison between mean values of microgap of Group I (Ni-Cr) and Group II (Co-Cr) samples at implant-cast abutment interface before cyclic loading using Independent ‘t’-Test

GROUP	No. of samples	Mean Microgap (µm)	Standard Deviation	p - value
I (Ni-Cr)	10	2.7939	0.76515	0.458
II (Co-Cr)	10	2.4002	1.45310	

p - value > 0.05; significant at 5% level

Inference:

On statistical analysis using Independent ‘t’-Test to compare the mean microgap of Group I and II samples at the implant-cast abutment interface before cyclic loading, it was found that the mean microgap of Group I samples was greater than the mean microgap of Group II samples and the p - value was > 0.05, denoting statistically insignificant difference between the two mean values.

Table VIII: Comparison between mean values of microgap of Group I (Ni-Cr) and Group II (Co-Cr) samples at implant-cast abutment interface after cyclic loading using Independent ‘t’-Test

GROUP	No. of samples	Mean Microgap (µm)	Standard Deviation	p - value
I (Ni-Cr)	10	0.1914	0.34999	0.697
II (Co-Cr)	10	0.2773	0.59159	

p - value > 0.05; significant at 5% level

Inference:

On statistical analysis using Independent ‘t’-Test to compare the mean microgap of Group I and II samples at the implant-cast abutment interface after cyclic loading, it was found that the mean microgap of Group I samples was lesser than the mean microgap of Group II samples and the p - value was > 0.05, denoting statistically insignificant difference between the two mean values.

Table IX: Overall comparison between mean values of microgap at implant-cast abutment interface of Group I (Ni-Cr) and Group II (Co-Cr) samples before and after cyclic loading

Groups Loading	Group I (Ni-Cr) (μm)	Group II (Co-Cr) (μm)	p-value
Before cyclic loading	2.7939	2.4002	0.458
After cyclic loading	0.1914	0.2773	0.697
p- value	0.000*	0.001*	

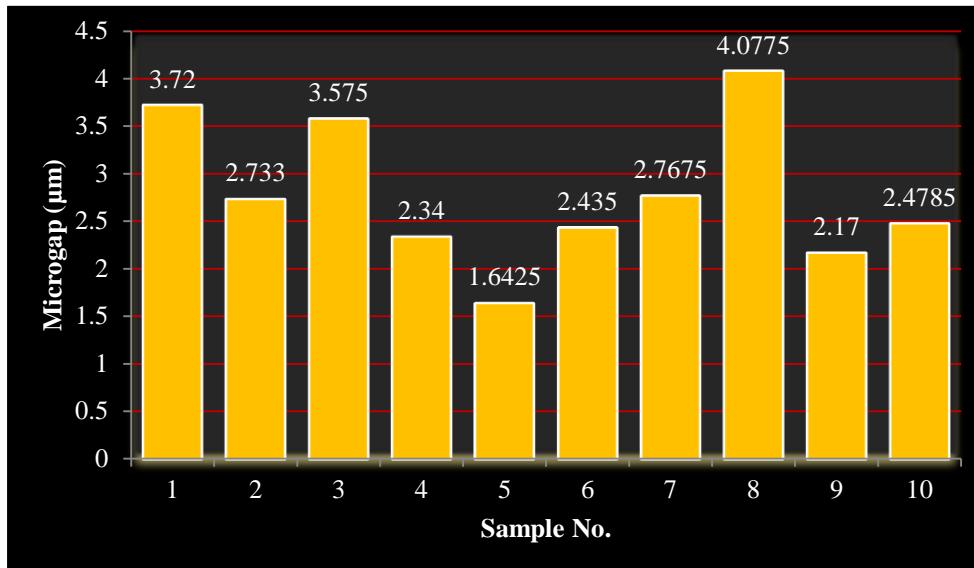
*p - value < 0.05; significant at 5% level.

Inference:

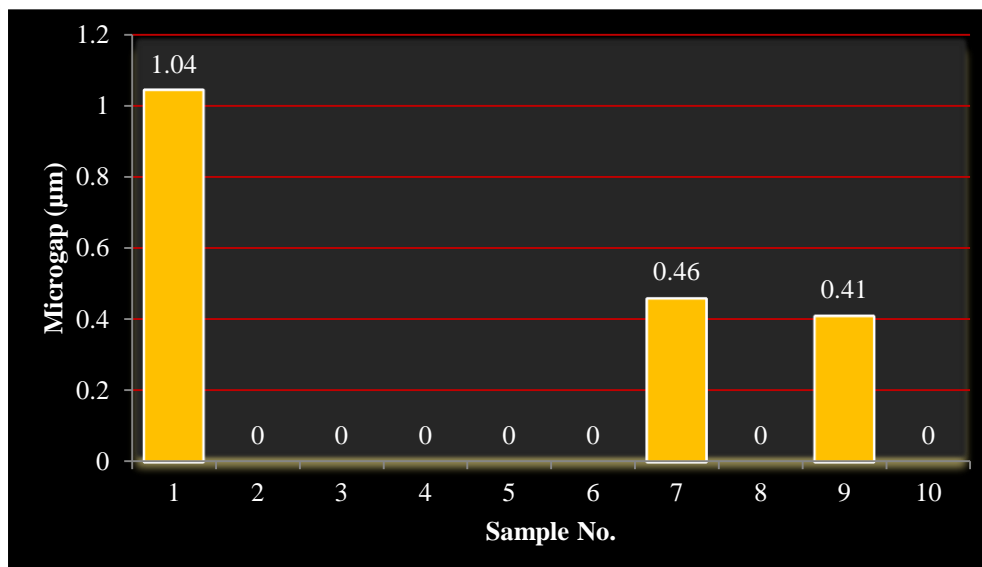
Statistical analysis with Independent ‘t’-test was used to compare the respective differences in mean microgap values of Group I and Group II samples before and after cyclic loading. The difference between the mean microgaps of Group I (Ni-Cr) and Group II (Co-Cr) samples before cyclic loading was found to be statistically insignificant (p-value > 0.05). Similarly, the difference between the mean microgaps of Group I (Ni-Cr) and Group II (Co-Cr) samples after cyclic loading was also found to be statistically insignificant (p-value > 0.05).

Statistical analysis with Paired 't'-test was used to compare the effects of cyclic loading on mean microgap values of Group I and Group II samples at the implant-cast abutment interface. The mean microgap values after cyclic loading were significantly lower than the mean microgap values before cyclic loading for both Group I (Ni-Cr) and Group II (Co-Cr) test samples (p-value < 0.05).

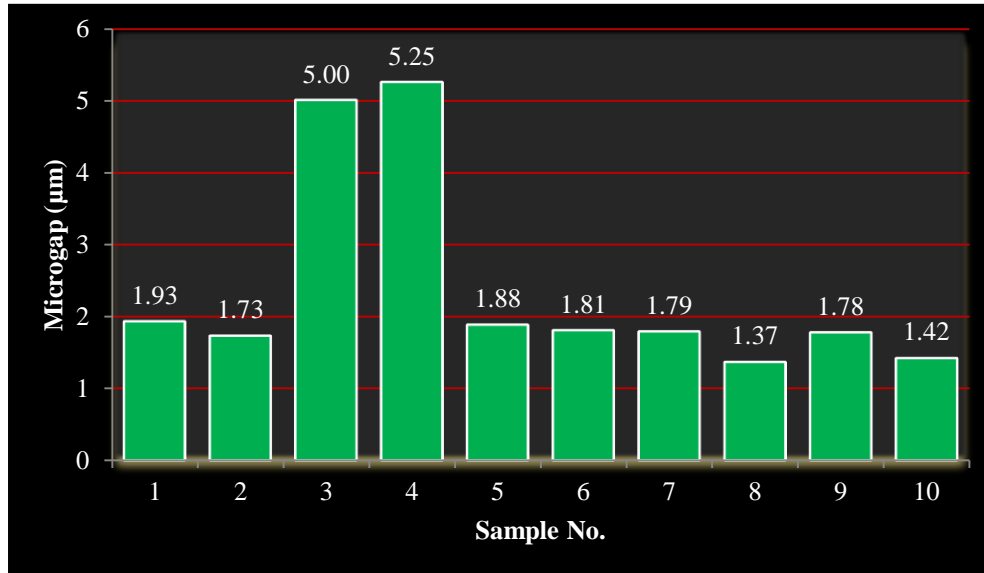
GRAPH I: Basic values of microgap at implant-cast abutment interface for Group I samples (Ni-Cr) before cyclic loading



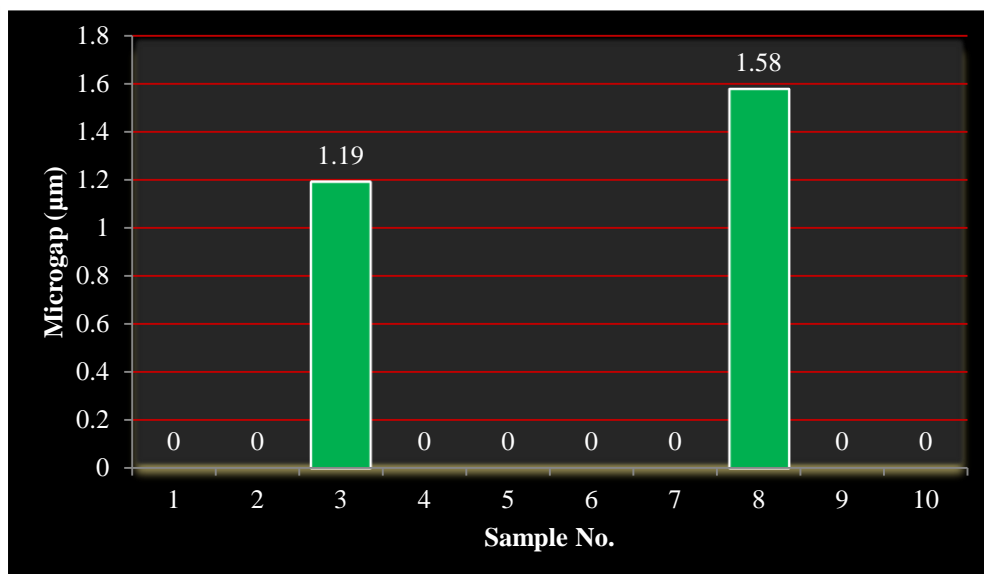
GRAPH II: Basic values of microgap at implant-cast abutment interface for Group I samples (Ni-Cr) after cyclic loading



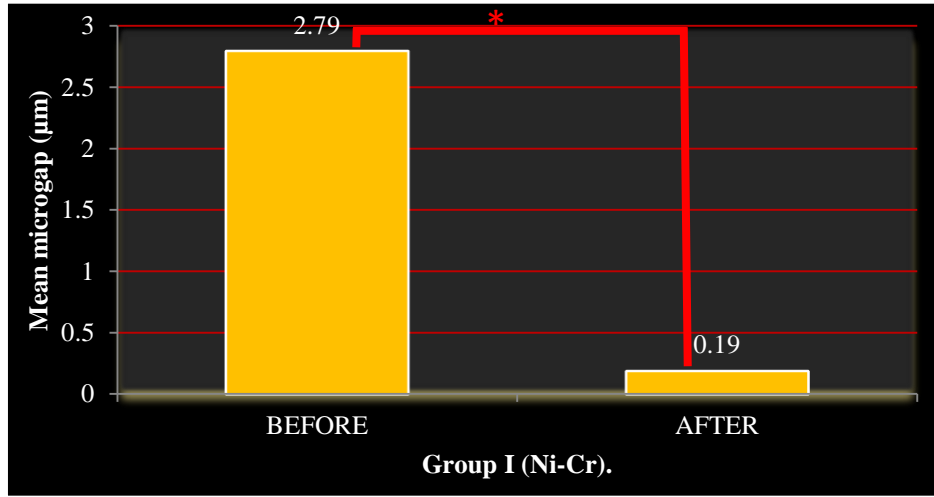
GRAPH III: Basic values of microgap at implant-cast abutment interface for Group II samples (Co-Cr) before cyclic loading



GRAPH IV: Basic values of microgap at implant-cast abutment interface for Group II samples (Co-Cr) after cyclic loading

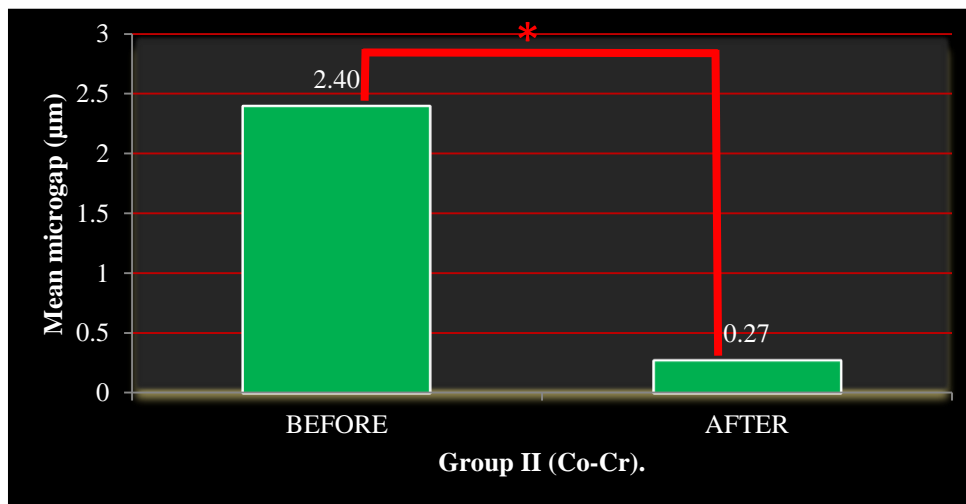


GRAPH V: Comparison between mean values of microgap at the implant-cast abutment interface of Group I samples (Ni-Cr) before and after cyclic loading



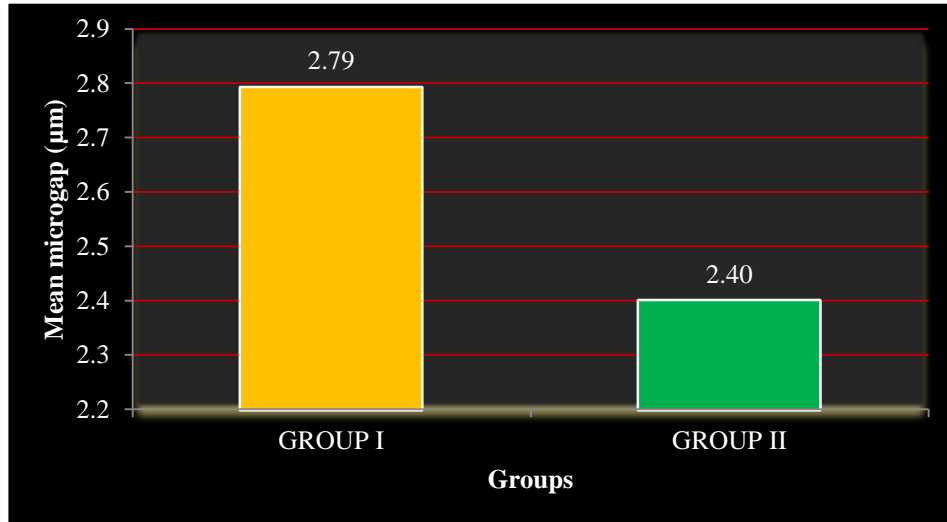
*Significant at 5% level

GRAPH VI: Comparison between mean values of microgap at the implant-cast abutment interface of Group II samples (Co-Cr) before and after cyclic loading



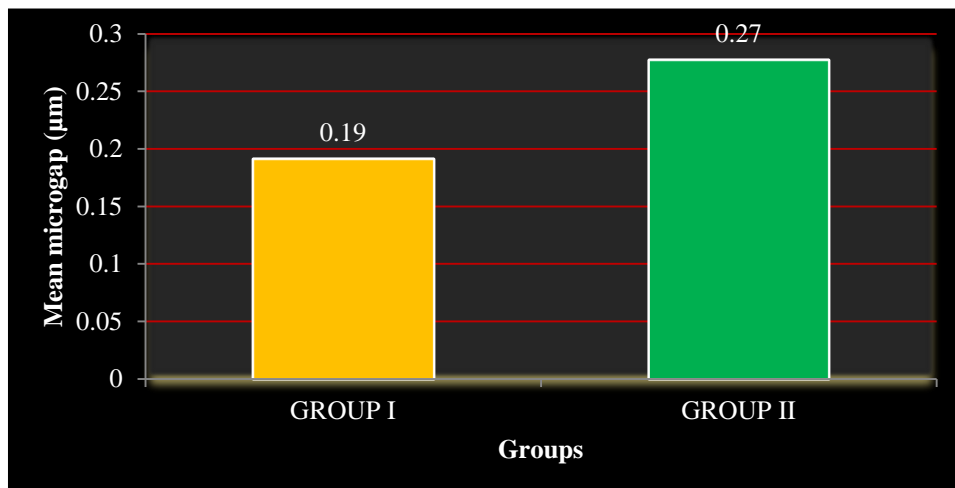
*Significant at 5% level

GRAPH VII: Comparison between mean values of microgap of Group I (Ni-Cr) and Group II (Co-Cr) samples at implant-cast abutment interface before cyclic loading



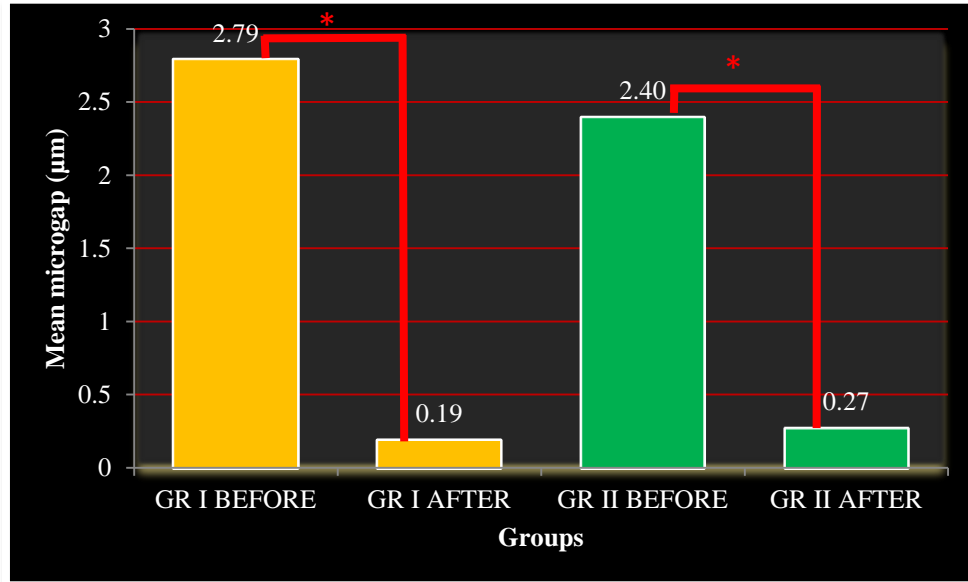
Not significant at 5% level

GRAPH VIII: Comparison between mean values of microgap of Group I (Ni-Cr) and Group II (Co-Cr) samples at implant-cast abutment interface after cyclic loading



Not significant at 5% level

GRAPH IX: Overall comparison between mean values of microgap at implant-cast abutment interface of Group I (Ni-Cr) and Group II (Co-Cr) samples before and after cyclic loading



* Significant at 5% level within groups

DISCUSSION

The present in-vitro study was conducted to comparatively evaluate the effect of cyclic load on the microgap at the implant-abutment interface, with the cast abutment-restorations fabricated using two different base metal alloys.

Osseointegrated titanium dental implants have been used extensively in oral rehabilitation for the replacement of one or more missing teeth, with survival rates over 90%.^{1,11,38,53} The treatment option of single-tooth implant supported restoration is now largely accepted with satisfactory outcomes from longitudinal studies reported in the literature.¹³

The main designs with endosteal dental implants that have emerged for such single-tooth prosthetic rehabilitation are the two-piece and single-piece implants. Of the two, the former is more popular owing to its versatility in a multitude of clinical situations and also because they can be individually loaded with different types of abutments.^{11,40} Two-piece dental implant consists of two separate components: the endosteal implant and the abutment carrying the prosthetic restoration connected by a screw joint.⁷ Implant restorations over such two-piece implants can be cement-retained, screw-retained, or a combination of both. Even though, cement-retained prostheses provide a less costly and simpler method of fabrication, their use in the anterior single-tooth situation may be restricted due to implant angulation and esthetic requirements.^{27,35}

The use of screw-retained implant prostheses in restoring completely and partially edentulous patients is well documented.^{2,35} They are advocated in partially edentulous situations to overcome angulation and esthetic problems.^{7,8} They provide the advantage of retrievability of restorations for reservicing and/or replacement of the restoration.³⁵ It is also reported that screw-retained prostheses have exhibited significantly smaller marginal opening at the implant-abutment interface as compared to cement-retained restorations.²⁷

In screw-retained restorations, the fastening screw provides a solid joint between the restoration and the implant abutment or between the restorations and the implant itself, for example, with UCLA abutments or UCLA-type plastic burnout patterns.³⁵

Although screw-retained crown protocol for a single-tooth two-piece implant, is well established, crown complications are common.^{10,27} The misfit at the implant-abutment interface and the integrity of the implant-abutment screw joint are factors that contribute towards these complications.^{10,15} The precision of fit begins at the junction of the implant and abutment placed on the implant.³⁰ This joint is also known as the implant-abutment interface. This can be either a butt-joint or a bevel joint.⁷ The contact between implant and abutment platform is a key factor, as it reduces the load over the abutment or prosthesis screw.⁸ Poor adaptation or misfit at the implant-abutment interface gives rise to a marginal gap between the implant and the abutment. Various

researchers have demonstrated the presence of microgap at the implant-abutment interface of two-piece dental implants.^{7,8,11,25,26,49} Imperfections related to casting of implant components, excessive torque during abutment placement (which may allow the distortion of its parts), and in addition the misfit between implant-cast abutment are factors that have been related to interface microgap origin.²³ The size of this microgap also plays a role in complications associated with screw joint integrity,¹⁵ which can be either biologic, mechanical or a combination of both.^{25,27} These complications can be controlled by reducing the misfit at the implant-abutment interface.^{7,8,22}

From a mechanical standpoint, screw-type connections (both external and internal hexagon types) rely on clamping the abutment to the top of the implant by a connecting screw, torqued to pre-determined values as established by the implant manufacturer.¹¹ This clamping force between two surfaces is maximized and most stable when no gaps are present between them. The success of a screwed connection is directly related to the preload reached during torque and its maintenance over time. Preload has been described as the tension generated in an abutment screw upon tightening and is a direct determinant of the clamping force. Misfit at the interface may lead to mechanical failures such as early loss of preload and screw loosening, abutment screw fracture, implant fracture and even prosthesis fracture and potentiate clinical implant failure.^{9,49}

This misfit also results in increased microleakage,²³ gingivitis and bone loss.^{20,39} It allows micro-organisms to penetrate and colonize even into the inner part of the implant,¹⁶ leading to periodontitis, progressive bone loss approximately 2 mm apical to the microgap²⁰ and eventually implant loss.^{16,47} Bacterial penetration has also been reported to occur under masticatory cycles.⁴⁶ Micro movements of the implant components during function may allow the initiation of a pumping effect, causing bacteria to move through the implant-abutment interface.³⁸ The microgap can be further enlarged under loading when the implant assembly components are subjected to eccentric forces. Thus bacterial colonization is impacted by multifactorial conditions like the precision fit between the implant components, torque forces when the components are connected and loading forces when the implants are in function.⁴⁷

Further, the geometry of the implant-abutment connection may also affect stresses generated from loading and these stresses may have a role in development of complications.³ Implant-abutment connection geometry can be broadly classified into external or internal connection.⁷ Internal hexagon connection has reported advantages over external connection design such as: (1) reduced vertical height from the implant platform to the top of the abutment; (2) distribution of lateral loading deep within the implant, leading to a better shielded abutment screw; and (3) long internal wall engagement that creates a stiff unified body to resist implant-abutment joint opening.^{7,49}

During function, clinical loading may result in micro-motion in stable implant-abutment screw joint, which contributes to screw loosening and increase in the microgap at the implant-abutment interface.¹⁵ The microgap at the implant-abutment interface may increase because of bending moments and consecutive fatigue and wear at the interface especially when loaded under eccentric forces. This is followed by the aforementioned mechanical and biologic sequelae.^{20,38,39,47} Majority of studies on the microgap at the implant-abutment interface have observed the interface in a static condition, not considering the chewing stresses.^{16,42} In-vitro cyclic loading of the implant-prosthesis assembly induces micro-motion of the joint components, which could wear down the microscopically rough areas of the contacting surfaces, thereby affecting joint stability. Fatigue or cyclic loading tests are intended to simulate components in function, which permits analysis of possible interaction between microgap and loading.^{8,11,15,23,25,26,49} Hence, in the present study, a cyclic loading test was included in the study design to simulate components in function and analyze possible interactions between implant-cast abutment interface and loading.

Commercially, pre-machined abutments are available in titanium alloy, noble metal alloys, base metal alloys, aluminium oxide alloys, zirconia and zirconia with titanium alloy connections.⁷ In order to address angulation and esthetic concerns, castable, plastic burnout patterns popularized by the UCLA abutment, that can be cast using various alloys are available.^{8,32} This burnout

pattern, fits directly on top of either the implant intra-orally or on the laboratory implant analogues, which are placed in the master cast. The plastic pattern is used to develop the wax pattern for the final restoration, which will connect directly to the implant restoration.³² These UCLA type castable abutments can be cast with noble metal alloys and base metal alloys.^{13,25,26,43} Noble metal alloys were the first to be used as castable material but with the development of economical materials for casting with significantly better mechanical properties, their use has decreased.¹⁹ Titanium alloys have exceptional mechanical properties and excellent biocompatibility. They provide excellent corrosion resistance to saline or acidic environments. Nevertheless, casting titanium alloys have a high production cost and are highly technique sensitive.⁴³ Other base metal alloys like Nickel-Chromium (Ni-Cr) and Cobalt-Chromium (Co-Cr) used in screw-retained implant supported restorations have comparable mechanical properties to that of titanium, with their modulus of elasticity being the best among all alloys used for cast restorations.^{5,26} These alloys also provide a low cost solution for screw-retained prosthesis,¹⁹ thereby reducing overall treatment costs and making it an affordable treatment option for many patients.

The microgap of premachined titanium abutment to the implant interface in a single-tooth implant situation has been documented in terms of precision of fit,⁸ as has been the microgap between single-tooth implant-cast abutments.^{8,13,25} Existing reports on cast abutments pertain mostly to noble

metal alloys and titanium alloys and few on other base metal alloys, such as Ni-Cr and Co-Cr alloys. There is limited documentation on the effect of cyclic load on microgap using abutments cast with Ni-Cr and Co-Cr alloys with an external connection design.¹³ However, studies on the effect of cyclic load on microgap using abutments cast with Ni-Cr and Co-Cr base metal alloys with an internal connection design are lacking. Therefore, the present study was conducted to evaluate the effect of cyclic load on the microgap at the implant-cast abutment interface of a screw-retained cast abutment-restoration, fabricated using two different base metal alloys, namely Ni-Cr and Co-Cr and measured by scanning electron microscope.

Unsterile, titanium implants were used in this study as titanium continues to be the most common material used for implant fixtures. Since this was an in-vitro study measuring only the effect of mechanical factors on the implant-cast abutment interface, it was assumed that an unsterile implant would suffice. The internal connection design was chosen for aforementioned reasons.

Autopolymerizing methyl methacrylate resin, which has a reported elastic modulus of 1.95 GPa, similar to that of trabecular bone⁵³ was used to embed the unsterile implant in custom-fabricated stainless steel blocks. Except 1mm at the crest module, the entire implant was submerged to allow easy visualization of the implant-cast abutment interface for making measurements.

In the present study, a screw-retained, anterior, maxillary single crown restoration was fabricated by waxing over a UCLA-type plastic burnout pattern. The pattern was contoured so as to facilitate easy placement and stabilization of the stylus of the custom-made cyclic loading machine.

The non-axial forces affecting the anterior maxilla causes higher stress concentrated along the facial and lingual surfaces of the implant-abutment interface.⁵³ The implant-abutment interface in this study was of butt joint design. Hence, in the present study, the cyclic loading was performed as 30° oblique loading, which not only better simulates the occlusal relationship of maxillary and mandibular incisors and the functional stresses along the long axis of the tooth, but also simulates the mechanical events occurring clinically at the implant-abutment interface in butt-joint designs. This was achieved by the use of a custom-made jig consisting of a platform and bolt.

A torque of 35 Ncm, is considered an optimum preload to maintain the screw-joint integrity, which maximizes the fatigue life of the screw and offers a reasonable degree of protection against loosening.^{49,53} This was also in line with the manufacturer's recommendation and hence this protocol was followed in the present study to connect the cast abutment-restorations to the implant.

Various methods to measure the microgap at the implant-abutment interface include scanning electron microscopy (S.E.M.),^{8,12,14,23,53} scanning

laser microscopy (S.L.M.),⁵⁰ optical microscopy,^{5,13} reflex microscopy, travelling microscopy, stereomicroscopy,²⁷ liquid strain gauges,²¹ gas permeability,⁴⁸ radiography,^{40,44} 3D micro-tomographic technique,³⁴ laser videography, and photogrammetric techniques.¹¹

S.E.M. measurements are a precise and well documented method for measurement of microgap.^{8,11,12,14,50,53} Microgap of butt-joint connections has been inspected by scanning electron microscopy,^{11,50} and was adopted for obtaining the microgap measurements in this study. The S.E.M. used in the present study has a working distance of 10 mm and a magnification of x5 to x3,00,000 and was adequate for observing the implant-cast abutment interface of test samples at x500. This magnification was chosen due to the clear visualization of the interface. Auto focus and auto alignment mode of the S.E.M. enabled visualization and measurements at the centre of the interface for each surface. This allows the use of repeatable measuring point, so that samples can be centred and measured both before and after cyclic loading. PC-SEM software along with Quartz PCI software was used to measure the microgap at the implant-cast abutment interface with a sensitivity of 1nm.

In the present study, a cyclic loading test was performed with a custom-made cyclic loading machine fabricated with specifications as reported in literature.^{23,49,53}

There is no standardization or consensus between previous studies regarding the applied forces for simulation. Forces in the range of 300 N, 100-150 N, 10-250 N, 20-200 N, 100-450 N, 50 N and 120 N have been used in different studies and also the mode (angle) of loading has varied. The loading frequencies also vary.^{13,15,18,21,28,41,49} Rack et al have quoted Mericske-Stern et al, stating that, a load of 110 N occurs on the abutment carrying the implant-supported restorations.⁴⁰ In the present study the test sample was cyclically loaded between 0-109 N to 1,50,000 cycles, simulating 6 months of function.

In the present study, the mean microgap of each test sample was measured both before and after cyclic loading. The microgap of each test sample was first calculated based on four measurements obtained, one for each surface, namely, facial, mesial, palatal and distal. All test samples of both test groups exhibited pre-load microgaps. The mean microgap value for each test group was then calculated.

The mean microgap for Group I test samples cast using Ni-Cr alloy before cyclic loading was found to be 2.7939 μm . The mean microgap for Group II test samples cast using Co-Cr alloy before cyclic loading was found to be 2.4002 μm . This microgap can be attributed to the casting procedures employed leading to differences between machined implant platform and cast abutment surface. Previous research using plastic burnout abutments cast with using gold, Ni-Cr alloy, Co-Cr alloy and cast titanium have shown microgap values ranging from 7 μm to 29.9 μm before cyclic loading.^{5,13,25} Both the

mean microgap values of both Group I and II in this study, were well below this range, as well as that of the clinically acceptable range (less than 10 μm).^{6,20,42} These results are indications of acceptable and standardized procedures adopted for fabrication of test samples.

Following cyclic loading, all the samples were subjected to visual and tactile inspection to check for deformation and/or cast abutment-restoration loosening. None of the twenty test sample employed in the present study exhibited any of the above, following which the microgap measurements were done. In the present study, the mean microgap for Group I test samples cast using Ni-Cr alloy after cyclic loading was found to be 0.1914 μm . The mean microgap for Group II test samples cast using Co-Cr alloy after cyclic loading was found to be 0.2773 μm . There was a statistically significant ($p < 0.05$) decrease in the mean microgap values after cyclic loading respectively, for both test groups in the present study. Scientific literature regarding microgap evaluation after cyclic loading of screw-retained abutment restorations cast using Ni-Cr or Co-Cr alloys is lacking. Previous studies on the effect of cyclic loading on premachined titanium abutments with either external or internal hexagon connections have demonstrated an increase in mean post-load microgap values.¹³ Similarly, De Jesus Tavares et al¹³ reported an increase in microgap values of about 5 μm after cyclic loading with cast-on gold abutments. Hoyer et al²¹ found an increase in microgap value in the range of 10 μm to 15 μm after 1,00,000 cycles of loading with the use of premachined

gold abutments. However, interestingly the same study reported a reduction in microgap value after 5,00,000 cycles. These limited studies, which evaluated the effect of cyclic loading and varying abutment materials on the microgap at the implant-abutment interface, reveal that the mechanical properties of the abutment material and probably also the duration of loading influences the fit at the implant-abutment interface.⁵³ Yuzugullu et al⁵³ compared the post-load mean microgap values between premachined titanium and custom machined alumina and zirconia abutments. Premachined titanium abutments exhibited a marginal increase in microgap only on the palatal side with no change on the other three sides, which was statistically insignificant. In contrast, they reported a marginal decrease in mean microgap values for custom-machined alumina and zirconia abutments after loading. The authors attributed this decrease in microgap to wear between contacting surfaces due to loading. Fretting wear occurs when repeated cyclic loading induces surface and subsurface breakup, resulting in loss of material. Fretting may have resulted in mating surfaces of both the abutment and implant surface to move closer. Even though the abutment screw might have ‘backed off’, the wear could have resulted in the surfaces settling towards each other, resulting in decrease of microgap. The findings in the present study are in line with those reported by Yuzugullu et al. Although the abutment materials employed here are different from their study, the same extrapolation can be drawn to interpret the results of the present study. Debris, an indicator of this wear, was evident at the

implant-cast abutment interface in the S.E.M. images after cyclic loading (Fig.44&45). However, this correlation needs further investigations.

Further, these authors also evaluated that there was no significant difference in the post load behavior between abutment materials i.e., the decrease in microgap values exhibited by different materials was similar. This is also in line with findings in the present study where both inter-group pre-load and post-load comparisons are not significantly different between both the test groups. Thus it can be reasonably assumed that both the alloys exhibit similar behavior during fabrication and when subjected to loading.

In the present study, even though our results showed the presence of gaps during the S.E.M. observation of the interface, caution must be taken when only this technique is considered as a method to evaluate the fit of the joint, since variations in gap sizes have been shown to occur along the implant radius in cross-sectional observations of this interface.^{11,33,53}

Although, these alloys appear satisfactory from a mechanical standpoint, biocompatibility issues remains. As 10% to 20% of the population is hypersensitive to Ni-based restorations, release of Ni ions in the surrounding tissues is a major concern. This release of ions occurs due to both occlusal wear as also due to corrosion in an acidic oral environment. Co-Cr alloys have shown to be more corrosion-resistant and hence superior than Ni-Cr alloys.⁴³ Hence, choice of cast abutment material can be based on individual operator's preference in correlation with individual clinical requirement and the

biocompatibility data available with respect to these alloys. Further studies that focus on these parameters simulating clinical conditions are required.

One of the limitations of the present study was that only a 6-month simulation of cyclic loading was performed. A longer loading period may affect the implant-cast abutment interface differently. The effect of cyclic loading on other mechanical parameters like reduction in preload, screw loosening, screw fracture, changes in platform surface characteristics and on biologic parameters like microbial leakage were not concomitantly evaluated. The effect of cyclic loading on the above parameters along with microgap assessment can be the basis of future studies. The cyclic loading was also performed under dry conditions. Corrosion fatigue performance of Ni-Cr and Co-Cr in saline environments at physiological temperatures, is of particular interest.⁴³ Therefore, future studies should also verify if the aging process causes critical damage to Ni-Cr or Co-Cr restorations.

Further research evaluating the effect of cyclic loading on the above parameters of castable abutments including other castable alloys for internal hexagon connections are recommended. Since there is no scientific support for the clinical belief that misfit alone contributes to clinical problems, in vivo studies regarding bone response to misfit can also be evaluated. More studies assessing the horizontal and rotational misfit as well as stress transfer of Ni-Cr and Co-Cr restorations are likely to provide better information regarding their clinical use and enhance the results obtained with the present study.

CONCLUSION

The following conclusions were drawn from the results obtained in the present in-vitro study, which was conducted to comparatively evaluate the effect of cyclic load on the microgap at the implant-abutment interface, with the cast abutment-restorations fabricated using two different base metal alloys. The microgap measurements were done by scanning electron microscopy.

1. The mean microgap at the implant-abutment interface of cast abutment-restorations fabricated using Nickel-Chromium (Ni-Cr) (Group I) before cyclic loading was found to be 2.7939 μm .
2. The mean microgap at the implant-abutment interface of cast abutment-restorations fabricated using Ni-Cr (Group I) after cyclic loading was found to be 0.1914 μm .
3. The mean microgap at the implant-abutment interface of cast abutment-restorations fabricated using Cobalt-Chromium (Co-Cr) (Group I) before cyclic loading was found to be 2.4002 μm .
4. The mean microgap at the implant-abutment interface of cast abutment-restorations fabricated using Co-Cr (Group I) after cyclic loading was found to be 0.2773 μm .
5. On comparison, the mean microgap values at the implant-abutment interface of cast abutment-restorations fabricated using Ni-Cr alloy, after cyclic loading (0.1914 μm) was lower than the mean microgap

value before cyclic loading (2.7939 μm) and their difference was found to be statistically **significant** ($p - \text{value} < 0.05$).

6. On comparison, the mean microgap value at the implant-abutment interface of cast abutment-restorations fabricated using Co-Cr alloy, after cyclic loading (0.2773 μm) was lower than the mean microgap value before cyclic loading (2.4002 μm) and their difference was found to be statistically **significant** ($p - \text{value} < 0.05$).
7. On comparison, the mean microgap values at the implant- abutment interface of cast abutment-restorations fabricated using Ni-Cr alloy (Group I - 2.7939 μm) and Co-Cr alloy (Group II - 2.4002 μm) before cyclic loading was found to be statistically **insignificant** ($p - \text{value} > 0.05$).
8. On comparison, the mean microgap values at the implant- abutment interface of cast abutment-restorations fabricated using Ni-Cr alloy (Group I - 0.1914 μm) and Co-Cr alloy (Group II - 0.2773 μm) after cyclic loading was found to be statistically **insignificant** ($p - \text{value} > 0.05$).
9. On overall comparison, the respective differences between the mean microgaps at the implant-abutment interface of Ni-Cr (Group I) and Co-Cr (Group II) screw-retained cast abutment-restorations, both before and after cyclic loading were found to be statistically **insignificant**. Cyclic loading had a **significantly** decreasing effect on

the microgap with both Ni-Cr (Group I) and Co-Cr (Group II) screw-retained cast abutment-restorations and these were within the clinically acceptable range of 10 μm .

SUMMARY

The present in-vitro study was conducted to comparatively evaluate the effect of cyclic load on the microgap at the implant-abutment interface, with the cast abutment-restorations fabricated using two different base metal alloys.

Twenty titanium implants were placed individually into autopolymerizing acrylic resin in custom stainless steel blocks and randomly divided into two groups of ten each. In Group I, ten screw-retained cast abutment-restorations obtained with Nickel-Chromium (Ni-Cr) alloy were connected to their corresponding implants and torqued to 35 Ncm. In Group II, ten screw-retained cast abutment-restorations obtained with Cobalt-Chromium (Co-Cr) alloy were similarly connected to their corresponding implants. The screw access hole was then sealed with light cure composite resin. The facial, mesial, palatal and distal surfaces of each test sample were labeled as A, B, C and D respectively.

Scanning electron microscope was employed to quantify the microgap at the implant-cast abutment interface individually for each test sample. One measurement each was obtained for four surfaces (A, B, C and D), of each test sample. The mean microgap for each sample and then for each group was obtained. Cyclic loading was performed for each sample individually at an angulation of 30° and subjected to cyclic loads simulating 6 months of function. Following cyclic loading, the microgap was again measured and

mean microgap calculated for each sample and then for each group in a similar manner as mentioned previously. The data obtained from the study was tabulated and statistically analyzed.

The mean microgap at the implant-cast abutment interface for both Group I (Ni-Cr screw-retained cast abutment-restoration) and Group II (Co-Cr screw-retained cast abutment-restoration) test samples was significantly lower after cyclic loading than the mean microgap before cyclic loading. This may be attributed to possible fretting wear of test samples due to cyclic loading.

On comparison, the respective differences between the mean pre and post cyclic load microgap measurements for both test groups were statistically insignificant. This was suggestive of similar behavior between both Ni-Cr and Co-Cr alloys. Hence, choice of cast abutment-restoration material can be based on individual operator's preference in correlation with clinical requirements and biocompatibility data available with respect to these alloys.

In this in-vitro study, the mean values of microgap obtained were less than 10 μm for screw-retained cast abutment-restorations, fabricated using Ni-Cr and Co-Cr alloy samples before and after cyclic loading which is in tune with those obtained in previous studies and considered to be within the clinically acceptable range.^{30,48,53}

Further investigations including longer loading periods, larger sample size and combined evaluations with other mechanical and biological parameters are recommended to enhance the results obtained with the present study.

BIBLIOGRAPHY

1. **Alberktsson T.** A multicenter report on osseointegrated oral implants. *J Prosthet Dent* 1988;60:75-84.
2. **Alberktsson T, Zarb G, Worthington P, Eriksson AR.** The long-term efficacy of currently used dental implants: A review and proposed criteria of success. *Int J Oral Maxillofac Implants* 1986;1:11-25.
3. **Asvanund P, Morgano SM.** Photoelastic stress analysis of external versus internal implant-abutment connections. *J Prosthet Dent* 2011;106:266-271.
4. **Barbosa GAS, Bernardes SR, das Neves FD, Fernandes Neto AJ, de Mattos Mda G, Ribeiro RF.** Relation between implant/abutment vertical misfit and torque loss of abutment screws. *Braz Dent J* 2008;19:358-363.
5. **Barbosa GAS, das Neves FD, de Mattos Mda G, Rodrigues RCS, Ribeiro RF.** Implant/abutment vertical misfit of one-piece cast frameworks made with different materials. *Braz Dent J* 2010;21:515-519.
6. **Barbosa GAS, Simamoto Junior PC, Fernandes Neto AJ, Mattos MDGCD, Neves FDD.** Prosthetic laboratory influence on the vertical misfit at implant/UCLA abutment interface. *Braz Dent J* 2007;18:139-143.

7. **Binon PP.** Implants and components: Entering the new millennium. *Int J Oral Maxillofac Implants* 2000;15:76-94.
8. **Byrne D, Houston F, Cleary R, Claffey N.** The fit of cast and machined implant abutments. *J Prosthet Dent* 1998;80:184-92.
9. **Cibirka RM, Nelson SK, Lang BR, Rueggeberg FA.** Examination of implant-abutment interface after fatigue testing. *J Prosthet Dent* 2001;85:268-75.
10. **Creugers NHJ, Kreulen CM, Snoek PA, De Kanter RJAM.** A systematic review of single-tooth restorations supported by implants *J of Dent* 2000;28:209-217.
11. **Coelho AL, Suzuki M, Dibart S, Da Silva N, Coelho PG.** Cross-sectional analysis of the implant-abutment interface. *J Oral Rehab* 2007;34:508-16.
12. **Cunha TDMAD, Araujo RPCD, Rocha PVBD, Amoedo RMP.** Comparison of fit accuracy between procera custom abutments and three implant systems. *Clin Implant Dent Relat Res* 2010;14:772-777.
13. **De Jesus Tavares RR, Bonachela WC, Xible AA.** Effect of cyclic loading on vertical misfit of prefabricated and cast implant single abutment. *J Appl Oral Sci* 2011;19:16-21.
14. **Dellow AG, Driessen CH, Nel HJC.** Scanning electron microscopy evaluation of the interfacial fit of interchanged components of four dental implant systems. *Int J Prosthodont* 1997;10:216-221.

15. **Gratton DG, Aquilino SA, Stanford CM.** Micromotion and dynamic fatigue properties of the dental implant-abutment interface. *J Prosthet Dent* 2001;85:47-52.
16. **Gross M, Abramovich I, Weiss EI.** Microleakage at the abutment-implant interface of osseointegrated implants: A comparative study. *Int J Oral Maxillofac Implants* 1999;14:94-100.
17. **Guimaraes MP, Nishioka RS, Bottino MA.** Analysis of implant/abutment marginal fitting. *Pos-Grad Rev Fac Odontol Sao Jose dos Campos* 2001;4:12-19.
18. **Hecker DM, Eckert SE.** Cyclic loading of implant-supported prostheses: Changes in component fit over time. *J Prosthet Dent* 2003;89:346-51.
19. **Hegde C, Prasad KD, Deepamala S, Hegde R.** Implant restoration materials: An overview 2010;1:43-48.
20. **Hermann JS, Schoolfield JD, Schenk RK, Buser D, Cochran DL.** Influence of the size of the microgap on crestal bone changes around titanium implants. A histometric evaluation of unloaded non-submerged implants in canine mandible. *J Periodontol* 2001;72:1372-1383.
21. **Hoyer SA, Stanford CM, Buranadham S, Fridrich T, Wagner J, Gratton D.** Dynamic fatigue properties of the dental implant-abutment interface: Joint opening in wide-diameter versus standard-diameter hex-type implants. *J Prosthet Dent* 2001;85:599-607.

22. **Jaime AP, de Vasconcellos DK, Mesquita AM, Kimpara ET, Bottino MA.** Effect of cast rectifiers on the marginal fit of UCLA abutments. *J Appl Oral Sci* 2007;15:169-74.
23. **Jansen VK, Conrads G, Richter EJ.** Microbial leakage and marginal fit of the implant-abutment interface. *Int J Oral Maxillofac Implants* 1997;12:527-540.
24. **Kano SC, Binon P, Bonfante G, Curtis DA.** Effect of casting procedure on screw loosening in UCLA-type abutments. *J Prosthodont* 2006;15:77-81.
25. **Kano SC, Binon PP, Curtis DA.** A classification system to measure the implant-abutment microgap. *Int J Oral Maxillofac Implants* 2007;22:879-885.
26. **Kano SC, Bonfante G, Hussne R, Siqueira AF.** Use of base metal casting alloys for implant framework: Marginal accuracy analysis. *J Appl Oral Sci* 2004;12:337-343.
27. **Keith SE, Miller BH, Woody RD, Higginbottom FL.** Marginal discrepancy of screw-retained and cemented metal-ceramic crowns on implant abutments. *Int J Oral Maxillofac Implants* 1999;14:369-378.
28. **Khraisat A, Hashimoto A, Nomura S, Miyakawa O.** Effect of lateral cyclic loading on abutment screw loosening of an external hexagon implant system. *J Prosthet Dent* 2004;91:326-334.
29. **Laney WR, Jemt T, Harris D, Henry PJ, Krogh PHJ, Polizzi G, Zarb GA, Herrmann I.** Osseointegrated implants for single-tooth

replacement: Progress report from a multicenter prospective study after 3 years 1994;9:49-54.

30. **Lang LA, Sierralta M, Hoffensperger M, Wang RF.** Evaluation of the precision of fit between the procera custom abutment and various implant systems. *Int J Oral Maxillofac Implants* 2003;18:652-658.
31. **Lee JH, Frias V, Lee KW, Wright RF.** Effect of implant size and shape on implant success rates: A literature review. *J Prosthet Dent* 2005;94:377-381.
32. **Lewis SG, Llamas D, Avera S.** The UCLA abutment: A four-year review. *J Prosthet Dent* 1992;67:509-15.
33. **Lorenzoni FC, Coelho PG, Bonfante G, Carvalho RM, Silva NRFA, Suzuki M, Silva TL, Bonfante EA.** Sealing capacity and SEM observation of implant-abutment interface. *Int J Dent* 2011;Jul 2 Epub 2011.
34. **Meleo D, Baggi L, Girolamo MD, Carlo FD, Pecci R, Bedini R.** Fixture-abutment connection surface and micro-gap measurements by 3D micro-tomographic technique analysis. *Ann Ist Super Sanita* 2012;48:53-58.
35. **Michalakis KX, Hirayama H, Garefis PD.** Cement-retained versus screw-retained implant restorations: A critical review. *Int J Oral Maxillofac Implants* 2003;18:719-728.
36. **Misch CE, Perel ML, Wang HL, Sammartino G, Galindo-Moreno P, Trisi P, Steigmann M, Rebaudi A, Palti A, Pikos MA, Schwartz-**

- Arad D, Choukroun J, Gutierrez-Perez JL, Marenzi G, Valavanis DK.** Implant success, survival and failure: The international congress of oral implantologists (ICOI) Pisa consensus conference. *Implant Dent* 2008;17:5-15.
37. **Moraes LMC, Rossetti PHO, Rossetti LMN, Pedreira APRDV, Valle ALD, Bonachela WC.** Marginal fit at cylinder-abutment interface before and after overcasting procedure *J Appl Pral Sci* 2005;13:366-371.
38. **Nascimento C, Miani PK, Pedrazzi V, Goncalves RB, Ribeiro RF, Faria ACL, Macedo AP, Albuquerque Jr RF.** Leakage of saliva through the implant-abutment interface: In vitro evaluation of three different implant connections under unloaded and loaded conditions. *Int J oral maxillofac implants* 2012;27:551-560.
39. **Pieri F, Aldini NN, Marchetti C, Corinaldesi G.** Influence of implant-abutment interface design on bone and soft tissue levels around immediately placed and restored single-tooth implants: a randomized controlled clinical trial. *Int J Oral Maxillofac Implants* 2011;26:169-78.
40. **Rack A, Rack T, Stiller M, Riesemeier H, Zabler S, Nelson K.** In vitro synctron-based radiography of microcap formation at the implant-abutment interface of two-piece dental implants. *J. Synchrotron Rad* 2010;17:289–294.

41. **Ribeiro CG, Maia MLC, Scherrer SS, Cardoso AC, Wiskott HWA.** Resistance of three implant-abutment interfaces to fatigue testing. *J Appl Oral Sci* 2011;19:413-420.
42. **Ricomini Filho AP, de Freitas Fernandez FS, Straioto FG, da Silva WJ, Del Bel Cury AA.** Preload loss and bacterial penetration on different implant-abutment connection systems. *Braz Dent J* 2010;21:123-9.
43. **Roach M.** Base metal alloys used for dental restorations and implants. *Sent Clin N Am* 2007;51:603-627.
44. **Sharkey S, Kelly A, Houston F, O'Sullivan M, Quinn F, O'Connell B.** A radiographic analysis of implant component misfit. *Int J Oral Maxillofac Implants* 2011;26:807-815.
45. **Stanford CM, Brand RA.** Towards an understanding of implant occlusion and strain adaptive bone modeling and remodeling. *J Prosthet Dent* 1999;81:553-561.
46. **Steinebrunner L, Wolfart S, Bobmann K, Kern M.** In vitro evaluation of bacterial leakage along the implant-abutment interface of different implant systems. *Int J Oral Maxillofac Implants* 2005;20:875-881.
47. **Tesmer M, Wallet S, Koutouzis T, Lundgren T.** Bacterial colonization of the dental implant fixture-abutment interface: an in vitro study. *J Periodontol.* 2009;80:1991-7.

48. **Torres JH, Mechali M, Romieu O, Tramini P, Callas S, Cuisinier FJ, Levallois B.** Development of a new quantitative gas permeability method for dental implant-abutment connection tightness assessment. *Biomed Eng Online* 2011;14:10:28.
49. **Tsuge T, Hagiwara Y.** Influence of lateral-oblique cyclic loading on abutment screw loosening of internal and external hexagon implants. *Dent Mater J* 2009;28:373-381.
50. **Tsuge T, Hagiwara Y, Matsumura H.** Marginal fit and microgaps of implant-abutment interface with internal anti-rotation configuration. *Dent Mater* 2008;27:29-34.
51. **Vasconcellos DK, Bottino MA, Nishioka RS, Valandro LF, da Costa EMW.** The influence of different screw tightening forces on the vertical misfit of implant-supported frameworks. *J Appl Oral Sci* 2005;13:120-5.
52. **Yi JM, Lee JK, Um HS, Chang BS, Lee MK.** Marginal bony changes in relation to different vertical positions of dental implants. *J periodontal Implant Sci* 2010;40:244-248.
53. **Yüzügüllü B, Avcı M.** The implant-abutment interface of alumina and zirconia abutments. *Clin Implant Dent Relat Res* 2008;10:113-21.
54. **Zarb GA, Schmitt A.** The longitudinal clinical effectiveness of osseointegrated dental implants in anterior partially edentulous patients. *Int J Prosthodont* 1993;5:180-188.